The GABAergic Gudden's dorsal tegmental nucleus: A new relay for serotonergic regulation of sleep-wake behavior in the mouse

Marine Chazalon, Sylvie Dumas, Jean-François Bernard, Iman Sahly, François Tronche, Alban de Kerchove D'exaerde, Michel Hamon, Joëlle Adrien, Véronique Fabre, Patricia Bonnavion

▶ **To cite this version:**

Marine Chazalon, Sylvie Dumas, Jean-François Bernard, Iman Sahly, François Tronche, et al.. The GABAergic Gudden's dorsal tegmental nucleus: A new relay for serotonergic regulation of sleep-wake behavior in the mouse. Neuropharmacology, 2018, 138, pp.315-330. 10.1016/j.neuropharm.2018.06.014 . hal-02333927

HAL Id: hal-02333927
https://hal.science/hal-02333927

Submitted on 28 Oct 2019

HAL is a multi-disciplinary open access archive for the deposit and dissemination of scientific research documents, whether they are published or not. The documents may come from teaching and research institutions in France or abroad, or from public or private research centers.

L'archive ouverte pluridisciplinaire **HAL**, est destinée au dépôt et à la diffusion de documents scientifiques de niveau recherche, publiés ou non, émanant des établissements d'enseignement et de recherche français ou étrangers, des laboratoires publics ou privés.

Neuropharmacology 138 (2018) 315–330

Contents lists available at ScienceDirect

Neuropharmacology

journal homepage: www.elsevier.com/locate/neuropharm

The GABAergic Gudden's dorsal tegmental nucleus: A new relay for serotonergic regulation of sleep-wake behavior in the mouse

Marine Chazalon [a], Sylvie Dumas [b], Jean-François Bernard [c, d], Iman Sahly [d], François Tronche [d], Alban de Kerchove d'Exaerde [a], Michel Hamon [c, d], Joëlle Adrien [e], Véronique Fabre [d, 1, **], Patricia Bonnavion [a, c, 1, *]

[a] Laboratory of Neurophysiology, Université Libre de Bruxelles (ULB), ULB Neurosciences Institute, Brussels, Belgium
[b] Oramacell, 75006, Paris, France
[c] Sorbonne Paris Cité, Université Paris Descartes, Inserm, Centre de Psychiatrie et Neurosciences (CPN), 75014, Paris, France
[d] Sorbonne Universités, UPMC Univ Paris 06, Inserm, CNRS, Neuroscience Paris Seine (NPS), Institut de Biologie Paris Seine (IBPS), 75005, Paris, France
[e] Université Paris Descartes, VIFASOM, Hôtel-Dieu de Paris, 75004, Paris, France

ARTICLE INFO

Article history:
Received 22 August 2017
Received in revised form
28 May 2018
Accepted 10 June 2018
Available online 14 June 2018

Keywords:
Serotonin
5-HT$_{1A}$ receptor
Sleep-wake cycle
Gudden dorsal tegmental nucleus
Lateral mammillary nucleus
Rabies viral tracing

ABSTRACT

Serotonin (5-HT) neurons are involved in wake promotion and exert a strong inhibitory influence on rapid eye movement (REM) sleep. Such effects have been ascribed, at least in part to the action of 5-HT at post-synaptic 5-HT$_{1A}$ receptors (5-HT$_{1A}$R) in the brainstem, a major wake/REM sleep regulatory center. However, the neuroanatomical substrate through which 5-HT$_{1A}$R influence sleep remains elusive. We therefore investigated whether a brainstem structure containing a high density of 5-HT$_{1A}$R mRNA, the GABAergic Gudden's dorsal tegmental nucleus (DTg), may contribute to 5-HT-mediated regulatory mechanisms of sleep-wake stages.

We first found that bilateral lesions of the DTg promote wake at the expense of sleep. In addition, using local microinjections into the DTg in freely moving mice, we showed that local activation of 5-HT$_{1A}$R by the prototypical agonist 8-OH-DPAT enhances wake and reduces deeply REM sleep duration. The specific involvement of 5-HT$_{1A}$R in the latter effects was further demonstrated by *ex vivo* extracellular recordings showing that the selective 5-HT$_{1A}$R antagonist WAY 100635 prevented DTg neuron inhibition by 8-OH-DPAT. We next found that GABAergic neurons of the ventral DTg exclusively targets glutamatergic neurons of the lateral mammillary nucleus (LM) in the posterior hypothalamus by means of anterograde and retrograde tracing techniques using cre driver mouse lines and a modified rabies virus.

Altogether, our findings strongly support the idea that 5-HT-driven enhancement of wake results from 5-HT$_{1A}$R-mediated inhibition of DTg GABAergic neurons that would in turn disinhibit glutamatergic neurons in the mammillary bodies. We therefore propose a Raphe→DTg→LM pathway as a novel regulatory circuit underlying 5-HT modulation of arousal.

© 2018 The Authors. Published by Elsevier Ltd. This is an open access article under the CC BY-NC-ND license (http://creativecommons.org/licenses/by-nc-nd/4.0/).

Abbreviations: 3V, 3rd ventricle; 4V, 4th ventricle; 7n, facial nerve; 8-OH-DPAT, 8-hydroxy-2-(di-n-propylamino)-tetraline; aCSF, artificial cerebrospinal fluid; AD, anterior dorsal thalamic nucleus; BSA, bovine serum albumin; cp, cerebral peduncle; DRc, caudal part of the dorsal raphe nucleus; DRi, interfascicular part of the dorsal raphe nucleus; DTg, Gudden's dorsal tegmental nucleus; f, fornix; fr, fasciculus retroflexus; GAD67, glutamate decarboxylase, 67 kDa type; HD, head direction cells; HDC, histidine decarboxylase; ISH, *in situ* hybridization; ml, medial lemniscus; LC, locus cœruleus; LDTg, laterodorsal tegmentum; LM, lateral mammillary nucleus; Mo5, motor trigeminal nucleus; MRN, median raphe nucleus; PDTg, posterodorsal tegmental nucleus; PHA-L, Phaseolus vulgaris-leucoagglutinin; pm, principal mammillary tract; PPTg, pedunculopontine tegmentum; py, pyramidal tract; scp, superior cerebellar peduncle; REM, rapid eye movement; TMN, tuberomammillary nucleus; VGLUT2, vesicular glutamate transporter 2.

* Corresponding author. Laboratory of Neurophysiology, Université Libre de Bruxelles, ULB Neuroscience Institute UNI, 808route de Lennik, 1070, Brussels, Belgium.
** Corresponding author. Sorbonne Universités, Site Pierre et Marie Curie, Inserm, CNRS, Neuroscience Paris Seine (NPS), Institut de Biologie Paris Seine (IBPS), 9Quai Saint Bernard, 75005, Paris, France.
E-mail addresses: veronique.fabre@upmc.fr (V. Fabre), pbonnavi@ulb.ac.be (P. Bonnavion).
[1] These two authors equally contributed to the work.

https://doi.org/10.1016/j.neuropharm.2018.06.014
0028-3908/© 2018 The Authors. Published by Elsevier Ltd. This is an open access article under the CC BY-NC-ND license (http://creativecommons.org/licenses/by-nc-nd/4.0/).

1. Introduction

Serotonergic neurons located in the raphe nuclei belong to the ascending arousal system that triggers cortical activation during wake. Indeed, most of serotonergic neurons discharge maximally during wake, decrease their firing rate during non-rapid eye movement (NREM) sleep and are silent during REM sleep (McGinty and Harper, 1976; Rasmussen et al., 1984; Sakai, 2011). As a result, extracellular 5-HT levels are higher during wake than during sleep both in the raphe nuclei and in brain areas targeted by 5-HT neurons (Portas et al., 2000). Importantly, enhancing 5-HT tone by systemic administration of selective serotonin reuptake inhibitors (SSRIs) has been repeatedly reported to inhibit REM sleep across species (Slater et al., 1978; Sommerfelt et al., 1987; Maudhuit et al., 1994; Monaca et al., 2003). In addition, recent findings have shown that 5-HT raphe neurons inhibit the pathological intrusion of REM sleep into wake in a mouse model of the sleep disorder narcolepsy (Hasegawa et al., 2017). Taken together, these observations suggest that 5-HT neurons promote cortical activation whilst impeding REM sleep onset during wake.

Serotonergic modulation of sleep/wake stages involves complex modalities of action and multiple receptors. Yet, a key role has been assigned to 5-HT_{1A} receptors (5-HT_{1A}R) in sleep regulation as knock-out mice that do not express these receptors exhibit higher amounts of REM sleep and altered REM sleep homeostasis (Boutrel et al., 2002). Furthermore, 5-HT_{1A}R underlie the SSRI-induced suppression of REM sleep. Indeed, the classical REM sleep deficits due to citalopram administration are not observed in 5-HT_{1A}R knock-out mice and are also markedly reduced after the pharmacological blockade of 5-HT_{1A}R in wild-type mice (Monaca et al., 2003). 5-HT_{1A}R are Gi/Go-protein-coupled receptors present on both somas and dendrites of serotonergic neurons in raphe nuclei (somatodendritic autoreceptors; Sotelo et al., 1990) and on target neurons receiving 5-HT projections (postsynaptic receptors; Kia et al., 1996; Riad et al., 2000). Through mediation of 5-HT inhibitory neurotransmission, stimulation of 5-HT_{1A}R *via* systemic administration of selective agonists has been consistently shown to markedly enhance wake and to decrease sleep with a main effect on REM sleep occurrence (Portas and Grønli, 2008). Whether these effects could be attributed to post-synaptic 5-HT_{1A}R or autoreceptors is still debated. Thus, contradictory effects were observed with local activation of 5-HT_{1A} autoreceptors in the dorsal raphe as it either enhanced (Bjorvatn et al., 1997) or did not modify (Sakai and Crochet, 2001) REM sleep. However, the effects of the 5-HT_{1A}R agonist ipsapirone on sleep persisted after the selective destruction of 5-HT neurons by the neurotoxin 5,7-dihydroxytryptamine (Tissier et al., 1993), which would rather suggest a primary role of post-synaptic 5-HT_{1A}R over autoreceptors in mediating 5-HT regulations of sleep/wake behavior.

Despite the established role of 5-HT_{1A}R in sleep regulation, the neural mechanisms and circuits by which the latter receptors are involved remain unclear. The brainstem is critical for the generation and maintenance of wake and REM sleep (Jouvet, 1962; Boissard et al., 2003; Lu et al., 2006; Cox et al., 2016). Multiple nuclei have been identified and involved in these functions but none of them express significant levels of post-synaptic 5-HT_{1A}R (Bonnavion et al., 2010). In contrast, we characterized a pontine nucleus containing a high density of 5-HT_{1A}R mRNAs, the Gudden's dorsal tegmental nucleus (DTg), which is mostly GABAergic (Bonnavion et al., 2010). This led us to investigate whether the latter nucleus is involved in the 5-HT_{1A}R-mediated inhibition of sleep in mice. For this purpose, we first confirmed the presence of 5-HT_{1A}R in GABAergic neurons of the DTg. Next, we analyzed the consequences of DTg lesions on sleep/wake states and investigated the role of 5-HT_{1A}R in the DTg on sleep regulation using local pharmacological injections of the 5-HT_{1A}R agonist 8-OH-DPAT. To further evaluate the specific involvement of 5-HT_{1A}R, we tested *ex vivo* the effects of 8-OH-DPAT on the activity of DTg neurons. Finally, we tracked the DTg connections throughout the brain to identify its downstream targets using anterograde and retrograde tracing methods including rabies-mediated trans-synaptic tracing and cre-based cell-type-specific targeting (Mebatsion et al., 1996; Kohara et al., 2014). Our findings reveal an unexpected contribution of the DTg in the 5-HT_{1A}R-mediated promotion of wakefulness through projections to glutamatergic neurons of the hypothalamic lateral mammillary nucleus (LM).

2. Materials and methods

2.1. Animals and surgeries

2.1.1. Animals and housing

In this study, VGLUT2-ires-cre knock-in (C57BL/6J background; The Jackson Laboratory; JAX:016963), transgenic 5-HT_{1A}-iCre/R26R (C57Bl/6J background; originally obtained from the colony of author FT; Sahly et al., 2007) and C57Bl/6J (reCentre d'élevage R. Janvier, Le Genest St Isle, France) adult (2-4 months-old) or juvenile (3-5 weeks-old) male mice were used. 5-HT_{1A}-iCre/R26R mice were obtained by crossing 5-HT_{1A}-iCre transgenic mice with R26R reporter mice harboring a LacZ transgene (Sahly et al., 2007). To avoid genetic drifts, mouse colonies were refreshed once a year with new commercial breeders. Mice were housed under standard conditions (12 h light-dark cycle, starting at 7:00 a.m.; 23 ± 1 °C ambient temperature; 60% relative humidity; food and water *ad libitum*). All experiments were performed in strict conformity with the European Union laws and policies for use of animals in neuroscience research (European Committee Council Directive 86/609/EEC), and with the Ethical Committee for Preclinical Research (nb 5) of the French Ministry of Research and High Education (articles R.214–124, R.214–125).

2.1.2. Electrolytic lesions

Adult male mice (n = 21; 8 weeks-old, body weight: 23–26 g) were anesthetized with ketamine/xylazine (K/X) [50 and 2 mg/kg, respectively, intraperitoneal (i.p.) injection] and placed in a stereotaxic apparatus. Electrolytic lesions of the DTg were made bilaterally by passing direct current (Constant current isolated stimulator, DS3, Digitimer Ltd, Welwyn Garden City, Hertfordshire, UK) with a monopolar electrode (100 μm in diameter, 0.2 mm exposed tip). Thirty pulses (1 s) of 60 μA were delivered at the following stereotaxic coordinates, from bregma (Franklin and Paxinos, 2008): 1) −5.0 mm anteroposterior (AP); ±0.25 mm lateral (L); −2.6 mm and −2.9 mm ventral from brain surface (V); 2) −5.4 mm AP; ±0.25 mm L; −2.8 mm and −3.1 mm V. No current was delivered through the electrode in the control group.

2.1.3. Intracerebral cannula implantations

As for electrolytic lesions, adult male mice (n = 17; 8 weeks-old, body weight: 23–26 g) were anesthetized with K/X and placed in a stereotaxic apparatus. A 26-gauge stainless steel cannula guide (Plastic one Inc, Roanoke, VA) with its tip aimed 1.0 mm above the DTg [from bregma (Franklin and Paxinos, 2008): −5.3 mm AP; 0.2 mm L; and −1.9 mm V] was anchored to the skull with dental acrylic cement. A dummy cannula was screwed in the cannula guide to avoid clogging.

2.1.4. Surgical procedure for sleep monitoring

After removal of the lesion electrode or implantation of the canula guide, mice were implanted with electroencephalogram (EEG), electrooculogram (EOG) and electromyogram (EMG)

electrodes for polygraphic recordings. EEG signals were recorded from two electrodes located on the frontal (from bregma: +2 mm AP; +2 mm L) and parietal (from lambda +1 mm AP; +2 mm L) cortices. EOG signals were recorded from two electrodes located subcutaneously on each side of the orbit, and EMG signals were recorded from two electrodes inserted in the neck musculature to record postural tone. All electrodes were soldered to a mini-connector (Antelec, La Queue en Brie, France). Dental acrylic cement was used to anchor the electrodes to the skull. Mice were allowed to recover for 7–10 days and then acclimated to the recording cables for a further 7 days in individual recording chambers.

2.2. Pharmacological treatment

For freely moving intracerebral drug administration, mice were first habituated for 7 days to daily gentle handling to minimize stress during injection. A 33-gauge stainless steel cannula was inserted into the implanted guide with a 1 mm protruding tip. At 10:00 a.m. (ZT 3), the 5-HT_{1A}R agonist 8-hydroxy-2-(di-n-propylamino)-tetralin (8-OH-DPAT, 20 μM; 250 pg in 50 nl of 0.9% sterile saline; Sigma, St. Louis, MO) or 0.9% sterile saline (50 nl) was infused at a flow rate of 50 nl/min. This amount of 8-OH-DPAT was chosen as lower doses (2.5 and 25 pg) did not significantly affect vigilance states (Supplementary Table 1). The cannula was left in place 3 min before mice were placed back in the recording chambers and recordings started.

2.3. Polygraphic recordings and analysis

EEG, EOG and EMG signals derived from the surgically implanted electrodes were amplified, sampled at 100 Hz (EOG) or 200 Hz (EMG and EEG), and digitized by an Embla Module (Medcare, Reykjavik, Iceland). All scoring was performed manually based on the visual signature of EEG, EOG and EMG waveforms of 5 s (microinjections) or 10 s (lesion) epochs to define wakefulness (WAKE), NREM or REM sleep following classical criteria (Boutrel et al., 2002) using sleep analysis Somnologica® software (Medcare, Reykjavik, Iceland). Amounts of time (also called amounts in the text) spent in WAKE, NREM and REM sleep were expressed as minutes per 1, 2 or 12 h intervals. NREM sleep latency was defined as time elapsed between the beginning of the recording and the first NREM sleep bout lasting at least 30 s. For REM sleep latency, we determined the time elapsed between the beginning of the first NREM sleep bout and the occurrence of the first REMS bout lasting at least 20 s.

2.4. Ex vivo electrophysiological recordings

2.4.1. Slice preparation

Male C57/Bl6 mice, 3–5 weeks-old, were anesthetized with halothane and killed by decapitation. Brains were removed and 220 μm coronal DTg slices were made using a vibratome (Leica VT1000S) in ice-cold (4 °C) dissection solution containing (in mM): choline chloride 140, KCl 2.5, NaH2 PO4 1.25, MgCl2 7, CaCl2 0.5, NaHCO3 25, glucose 14, saturated with 95% O2 and 5% CO2. Slices were transferred to the recovery chamber and incubated in artificial cerebrospinal fluid (aCSF) containing (in mM): NaCl 127, KCl 2.5, NaH2PO4 1.25, MgCl2 1, NaHCO3 26, D-glucose 10, CaCl2 2, bubbled with a mixture of 95% O2 and 5% CO2 at a pH of 7.3 (300–316 mOsm). After an initial recovery period of 1 h at 34 °C, slices were maintained at room temperature.

Individual slices were transferred to a thermoregulated (30–32 °C) chamber, maintained immersed with a nylon grid and continuously superfused at a rate of 1,5–2 ml/min with oxygenated aCSF. Neurons were identified with a 63 × water immersion objective from Zeiss Axioskop microscope (Axioskop 2FS Plus; 140 Zeiss, Oberkochen, Germany) with an infrared CCD camera (X-ST70CE, Hamamatsu Photonics KK, Hamamatsu, Japan) for extracellular or whole-cell recordings. For recording in mouse coronal slices, we chose sites strictly confined to the DTg (see *Anatomical validation* section below) avoiding DR midline neurons. When possible, confirmation of the neurons location was assessed with biocytin injection at the end of the recordings (N = 15). A first series of cells were recorded in loose-seal configuration, and a second series in whole-cell configuration to further examine basic characteristics of mouse DTg neurons. Borosilicate-glass patch electrodes [4–6 MΩ, (Hilgenberg GmbH, Malsfeld, Germany)] were filled with a solution containing (in mM): KMeSO3 125, KCl 12, CaCl2 0.022, MgCl2 4, HEPES 10, EGTA 0.1, Na2-phosphocreatine 5, Mg2-ATP 4, Na2-GTP 0.5 (pH of 7.2, 292 mOsm). An Ag/AgCl wire was used as reference electrode. Currents were recorded using an EPC-10 patch clamp amplifier (HEKA, Lambrecht, Germany) and PatchMaster acquisition software (HEKA).

2.4.2. Loose-seal patch recordings

Extracellular recordings of spontaneous action potentials were acquired in voltage clamp mode (0 mV) in loose-seal configuration. Signals were sampled at 20 kHz with a gain of 2 mV/pA and low-pass filtered at 2.9 kHz. Standard off-line detection of spontaneous action potentials was performed with Axograph X software (Axon Instruments Inc., Foster City, CA). For this analysis, we generated an action potential to scan the recording trace for similar waveforms. All matching events were stored and, if false positive events were detected, they were discarded on the basis of their amplitude or kinetics. Spontaneous neuronal activity was monitored during 5–10 min from the beginning of the recording during baseline aCSF perfusion for each neuron. Then, 8-OHDPAT (300 nM; Tocris Bioscience) and/or the 5-HT_{1A}R antagonist N-[2-[4-(2-methoxyphenyl)-1-piperazinyl]ethyl]-N-(2-pyridinyl) cyclohexane carboxamide (WAY 100635; 1 μM; Tocris Bioscience) were bath-applied by switching the perfusion system. Agonist and antagonist concentrations were used based on previous work showing specific involvement of 5-HT_{1A}R signaling (Loucif et al., 2006). Stock solutions were prepared in water at concentrations of 3 mM (8-OHDPAT) and 1 mM (WAY 100635), and stored at −20 °C then daily dissolved at desired experimental concentrations in aCSF. Three experimental protocols were performed involving: 1) 5–10 min aCSF baseline, then 10min perfusion of 8-OH-DPAT followed by 10–15min aCSF wash before applying WAY 100635 for 10 min, and 10 min of 8-OH-DPAT co-perfused with WAY 100635 (N = 3 cells); 2) 5–10 min aCSF baseline, then 5–10 min perfusion of 8-OH-DPAT followed by 5–10 min aCSF wash (N = 11 cells); and 3) 5–10 min aCSF baseline, then 10 min perfusion of WAY 100635 followed by 10 min co-perfusion of WAY 100635 + 8-OH-DPAT (N = 6 cells).

Firing rate of DTg neurons were calculated over 10-s bin intervals for statistical analysis and for neuronal response histogram representation of one responding DTg neuron in the complete pharmacological protocol (1) (Fig. 5B–C, mean ± S.E.M.). For analysis, we considered the mean baseline firing frequency in aCSF calculated over 2 min prior to 5-HT_{1A}R agonist application, and the mean firing rate during the maximum response to 8-OH-DPAT over a duration of 2 min. We calculated an averaged latency of 414 ± 42.5 s for 300 nM 8-OH-DPAT maximal response of DTg neurons. Here, we only considered neurons that showed a response to 8-OH-DPAT greater than baseline mean firing rate ± 2× S.E.M. (N = 10). To analyze the return to baseline values during the washout, we calculated the mean firing rate over a duration of 2 min after 5 min of aCSF wash. For the blocking protocol (3), we

considered the baseline mean firing frequency in aCSF calculated over 2 min prior to 5-HT_{1A}R antagonist, WAY 100635, application, and the mean firing rate calculated over the last 2 min under WAY 100635 before co-applying 8-OH-DPAT. We finally calculated the average firing rate over 2 min after 450 s of WAY 100635 + 8-OH-DPAT co-application (N = 9). Other analysis were performed with IgorPro 6.3 software (WaveMetrics, Portland, USA) using Patcher's Power Tools, NeuroMatic plugins and Microsoft Excel software.

2.4.3. Whole-cell recordings

Cells were first recorded in voltage-clamp mode at holding potential of −60 mV with a gain of 2 mV/pA and low-pass filtered at 2.9 kHz. Signals were sampled at 20 kHz. Passive membrane properties and access resistance were extracted from current traces recorded in response to a hyperpolarizing voltage pulse (200 ms) of −10 mV from holding potential. The membrane resistance was computed using the difference between the baseline current and the current at 40 ms during the voltage step. The integrated area under the transient from the same trace was used to determine membrane capacitance. Ten sweeps were averaged to remove noise.

In current-clamp mode, spontaneous action potential activity was monitored during 5 min at 0 pA during aCSF perfusion from the beginning of the recording. Signals were sampled at 10 kHz with a gain of 2 mV/pA. The detection and calculation of the firing rate was done after 1 min from the beginning of the recording during aCSF baseline, over the rest of the recording (4 min), and was identical as above, using the appropriate template. To measure the membrane potential, traces were filtered off-line at 2 Hz, and the amplitude of potential fluctuations was averaged over the duration of the recording. Series resistance was not compensated during the recordings and membrane potential values were corrected off-line with a liquid junction potential of 6.6 mV. If access resistance exceeded 30 MΩ, the recording was discarded.

2.4.4. Biocytin visualization

After electrophysiological recordings, 15 neurons were injected with biocytin (0.5%) added in the pipette internal solution to confirm their localization in the DTg. Slices containing one biocytin-injected DTg cell were immersed in an ice-cold fixative with 4% paraformaldehyde in 0.01 M phosphate-buffered saline (PBS) and kept overnight at 4 °C. After several washes in PBS, slices were permeabilized in a 0.1% Triton X-100 (Sigma-Aldrich) solution prepared in PBS (PBS-T) for 90 min. Slices were incubated in streptavidin-NL557 (1:2000 in PBS-T; NL999; R&D Systems) for 2 h under stirring at room temperature in the dark. Sections were rinsed 3 times in PBS during 10 min and mounted between slide and coverslip using Fluorsave mounting medium (Calbiochem).

Images were acquired on a Laser-Scanning Confocal System 228 (LSM 780; Zeiss, Oberkochen, Germany), mounted on an Axio observer Z1 inverted microscope (Zeiss, Oberkochen, Germany). He–Ne laser (543 nm) was used for excitation of Alexa Fluor 555, and emission signals were filtered. Images were acquired using Zen 2010 Software (Zeiss, Oberkochen, Germany) and processed in Fiji software.

2.5. Anatomical procedures

2.5.1. Anatomical validation

After completion of the recordings, both lesions and injection sites were checked. To do so, mice were deeply anesthetized: lesioned mice were transcardially perfused (see below), whereas animals that had been used for the pharmacological experiments received 50 nl of pontamine sky blue dye (2%) through the implanted cannula and were euthanized shortly after. Brains were removed and coronal brainstem sections were cut and Nissl counterstained.

We delineated nuclear boundaries using the Nissl staining (Kádár et al., 2009) to localize the DTg according to i) the *in situ* hybridization labeling of 5-HT_{1A}R mRNA (Fig. 1), ii) the anatomical characterization of the DTg subnuclei performed by Hayakawa and Zyo (1983), and iii) the mouse brain atlas (Franklin and Paxinos, 2008). The DTg is present on coronal brain sections extending from ~ −5.00 to −5.6 mm relative to bregma (Franklin and Paxinos, 2008). The 5-HT_{1A}R mRNA labeling within the DTg extends from ~ −5.1 to −5.4 mm relative to bregma, with highest signal density at −5.25 mm (Fig. 1). The DTg lies in the central grey matter, ventral to the 4th ventricle and dorsal to the medial longitudinal fasciculus, medial to the laterodorsal tegmentum (LDTg) and lateral to the caudal part of the DR. It is characterized by numerous stained perikarya clustered in an oval shape bordered by an area with fewer stained cells. The caudal DR is delineated by the presence of some large stained neurons located in the central grey matter, just ventral to the 4th ventricle and dorsal to the medial longitudinal fasciculus and medial to the left and right DTg.

The surface of DTg lesions was estimated as described by Bassett et al. (2007) for the rat. Briefly, brainstem sections were stained with Nissl staining as described above to delineate nuclear boundaries. The calculation of the lesioned surface was done for each mouse, blind of the sleep results, by manual delimitation of abnormal brain tissue, within counting boxes that encompassed the DTg coordinates as defined in the mouse brain atlas (Franklin and Paxinos, 2008). We analyzed 6 sections of 20 μm thickness per mouse, from −5.68 to −4.96 mm relative to bregma and the results were expressed in % of destruction of the DTg. Similar results were obtained with NeuN immunostaining (Supplementary Fig. 1).

2.5.2. Tracer microinjections

Under K/X anesthesia, a glass micropipette (20–30 μm outside tip diameter) filled with a solution (5%) of the anterograde tracer Phaseolus vulgaris-leucoagglutinin (PHA-L, Vector, Burlingame, CA) was lowered into the DTg [from bregma (Franklin and Paxinos, 2008): −5.3 mm, AP, 0.25 mm L, −2.95 mm V] of adult male C57Bl/6J mice (n = 7; 8-10 weeks-old, body weight: 23–26 g). Iontophoretic application of PHA-L was made by passing positive 2–6 μA current pulses (20 s per 30 s period) for 10 min. For retrograde tracing, iontophoretic injections of fluorogold (FG, 2%; Molecular Probes®, Invitrogen, Carlsbad, CA) were targeted to the LM [from bregma (Franklin and Paxinos, 2008): −2.4 mm AP, 0.8 mm L, and −4.5/-4.75 mm V] of adult male 5-HT_{1A}-iCre/R26R mice (n = 5; 8-10 weeks-old, body weight: 23–26 g) using glass micropipettes (25–40 μm outside tip diameter).

2.5.3. Viral tracing

Under K/X anesthesia, 400 nl of an adeno-associated (AAV1) Cre-dependent helper virus carrying the green fluorescent protein (GFP), rabies glycoprotein (RG) and avian-specific retroviral receptor TVA [AAV-synP-FLEX-sTpEpB packaged by the University of North Carolina vector core (Kohara et al., 2014),] was injected into the LM [from bregma (Franklin and Paxinos, 2008): −2.4 mm AP, 0.75 mm L, and −4.75 mm V] of VGLUT2-ires-cre mice (N= 4; 8-10 weeks-old male mice, body weight: 23–26 g). Ten days later, 500 nl of rabies viruses encoding mCherry or GFP (SADΔG GFP/mCherry; generous gift of Prof. K.K. Conzelmann) were injected into the same brain location. Brain tissue was removed and processed for dual *in situ* hybridization one week after the rabies virus injection.

2.5.4. Histological procedures

Under deep pentobarbital anesthesia (150 mg/kg i.p.), mice were transcardially perfused with a fixative solution of 4%

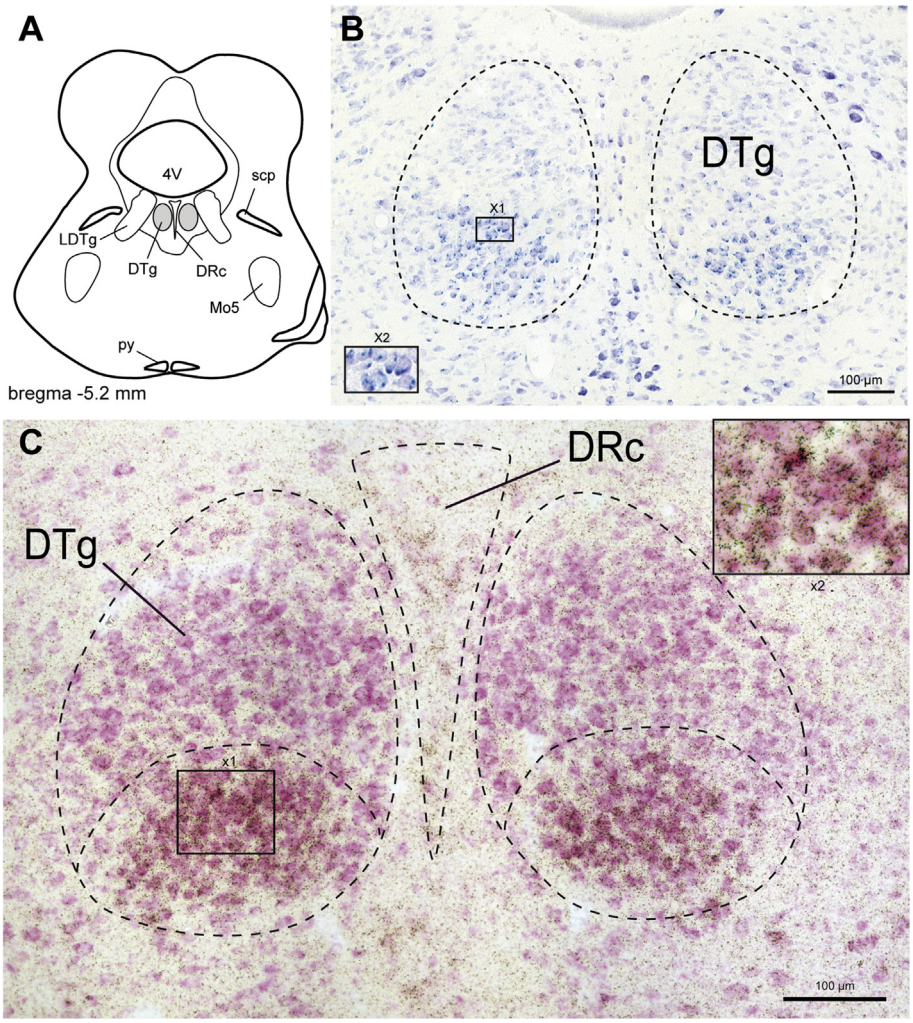

Fig. 1. 5-HT$_{1A}$R are expressed by GABAergic neurons of the DTg. **A**. Coronal view at the level of the DTg adapted from the stereotaxic atlas of Franklin and Paxinos (2008). The grey area corresponds to the DTg. **B**. High magnification image showing 5-HT$_{1A}$R mRNA expression (revealed by X-Gal staining, blue dots) in the ventral part of the DTg in a Nissl-stained coronal section of a 5-HT1A-iCre/R26R mouse. An example of 5-HT$_{1A}$R expressing neurons is shown in ×1 (and its two-fold magnified ×2) boxed area. **C**. Color photomicrograph of the DTg with double labeling for 5-HT$_{1A}$R (black grains) and GAD 67 (pink) mRNAs. Double labeled neurons are mainly observed in the ventral part of the DTg as shown in XI (and its two-fold magnified) ×2 box area. Distance from bregma is indicated in mm (from Franklin and Paxinos, 2008). (For interpretation of the references to color in this figure legend, the reader is referred to the Web version of this article.)

paraformaldehyde (Sigma) in PBS, pH 7.4; (Invitrogen Corporation, Carlsbad, CA). The brains were removed and post-fixed overnight. Then, three series of 30 or 35 µm-thick coronal brain sections were cut using a vibratome (VT-1000, Leica Microsystèmes, Rueil-Malmaison, France).

For β-galactosidase staining, one series of coronal sections were incubated overnight in X-Gal solution (5 mM potassium ferricyanide, 5 mM ferrocyanide, 2 mM $MgCl_2$, 0.02% NP-40, 0.01% sodium deoxycholate and 1 mg/ml X-Gal) at 37 °C. β-galactosidase activity was visualized as blue dot staining in the cytoplasm of labeled cells. All sections encompassing the DTg (N = 5) were visualized and photomicrographs were captured from a representative section.

For immunohistological staining in tracing experiments, coronal sections were incubated for 1 h in PBS containing 4% bovine serum albumin (BSA) and 0.1% Triton X-100 (PBST). They were then incubated overnight with either the goat polyclonal anti-PHA-L antibody at 1:2000 (Vector) or the rabbit polyclonal anti-fluorogold antibody at 1:40,000 (Chemicon, Temecula, CA, USA) in PBST. Secondary antibodies incubation (anti-goat or anti-rabbit IgG at 1:200; Vector) followed by additional steps for 3,3′-diaminobenzidine (DAB, Sigma) staining were performed as previously described (Bonnavion et al., 2010). Some sections were double stained for PHA-L using nickel enhancement, followed by immunostaining for histidine decarboxylase (HDC; rabbit anti-HDC antiserum; 1:3,000, Acris Antibodies Gmbh, Herford, Germany) without nickel, yielding black PHA-L fibers and brown HDC-immunoreactive cells. Stained sections were finally mounted on gelatin-coated slides, dehydrated, and coverslipped with Eukitt mounting medium (Kindler). Antibodies are described in Supplementary Table 2. The anti-HDC antiserum was made in rabbit against the rat enzyme. This anti-HDC antiserum stained C-terminally truncated isoforms (54 and 63 kDa) and the full length protein (73 kDa) in tissue homogenates from fetal rat liver (manufacturer's technical information; Dartsch et al., 1998). The distribution of HDC-positive neurons were in general agreement with those previously described in the rat brain (Ericson et al., 1987). Performance of the whole immunohistochemical procedure but without HDC primary antibodies yielded sections with no immunolabeling above background.

Dual *in situ* hybridization labeling for 5-HT$_{1A}$R and GAD67

(glutamate decarboxylase, 67 kDa type) mRNAs was performed as described previously (Bonnavion et al., 2010). Dual fluorescent *in situ* hybridization (FISH) labeling for GAD67, VGLUT2 or the green fluorescent protein (GFP) mRNAs was performed as described in Viereckel et al. (2016). Probes are described in Supplementary Table 2.

For image acquisition, photomicrographs were captured on different focal planes using a TRI CCD camera (JVC KY-F50; resolution 576 × 768 pixels) connected to an Olympus BX21 microscope using a 40 × objective, and were digitized by using a 3 × 8-bit color-scale Openlab software (Improvision, Coventry, U.K.). The images were then exported to Adobe Photoshop CS2 (version 9.0; Adobe Systems, Mountain View, CA) to mount adjacent digitized images as a final large-field high-resolution image and to adjust brightness and contrast. For FISH and immunohistofluorescence image acquisition, sections were scanned on a NanoZoomer 2.0-HT (Hamamatsu, Japan) at 20× resolution. Image microphotographs were analyzed using the ndp2.view software (Hamamatsu, Japan). For illustration purposes, the NanoZoomer images were exported in Tiff format using NDP viewer. Images were then corrected for contrast and cropped on Photoshop CS2.

2.6. Statistics

All data were analyzed using Prism 7.0 (GraphPad Software). Statistical significance was set at 0.05 for all procedures. Normality and homoscedasticity assumptions were verified prior to the use of any parametric tests (Shapiro-Wilk normality test and equality of variances *F-test*). In case of violation of any of these assumptions, standard transforms were applied to meet the above criteria. Statistics were performed with repeated measures two-way ANOVAs to test the significance between locus groups ("positive" or "negative" sites, see Results) and pharmacological conditions (saline or 8-OH-DPAT) for each time window (0–1 h, 1–2 h, 2–3 h) and for each vigilance state (wake, NREM, REM), and between lesion and time. These tests were followed by two-tailed unpaired t-test with Welch's correction when necessary or non-parametric Mann-Whitney tests between locus groups, lesioned and non-lesioned control groups. Ratio paired t-test and non-parametric two-tailed paired Wilcoxon test were also employed to assess the significance of the effects of pharmacological treatment on the different variables (amounts of time spent in sleep/wake states, latencies, bout mean durations, numbers of bouts). Statistical

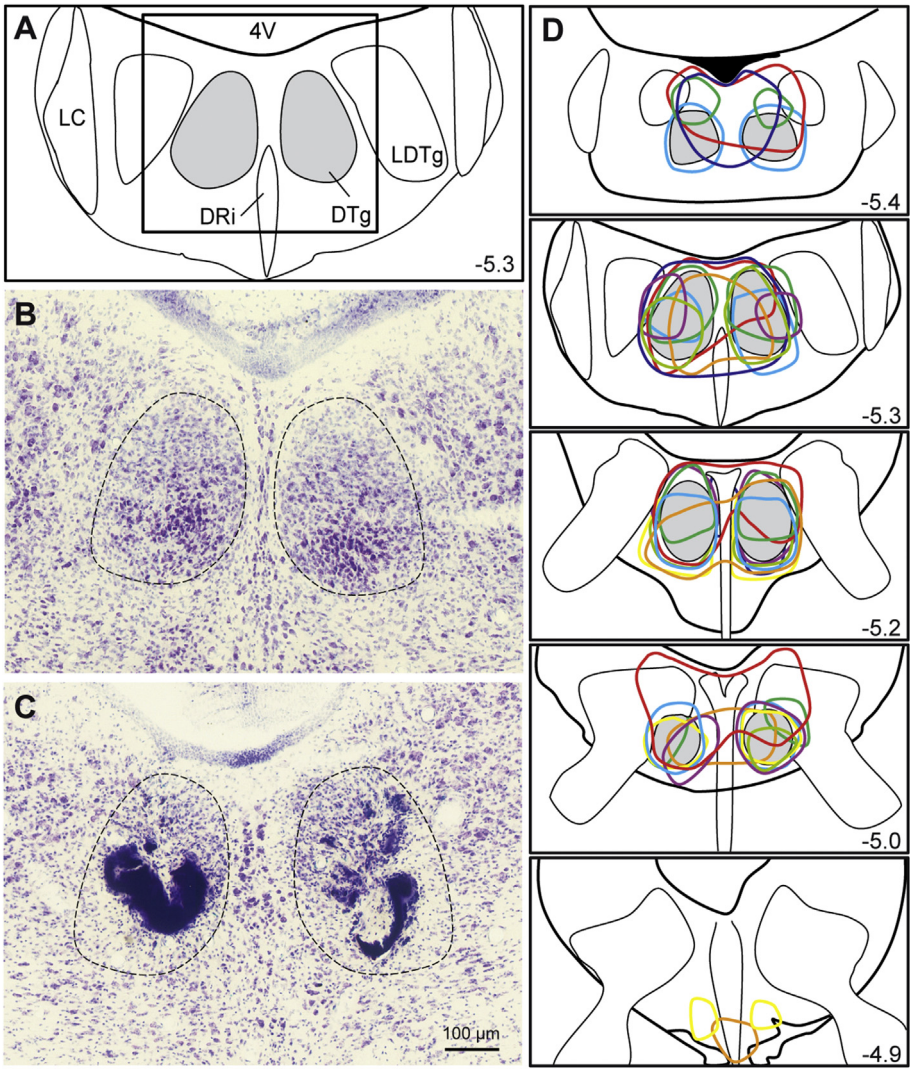

Fig. 2. Schematic drawings illustrating lesions of the DTg. **A**. Coronal view at the level of the DTg adapted from the stereotaxic atlas of Franklin and Paxinos (2008). The grey area corresponds to the DTg. **B-C**. Representative photomicrographs of Nissl-stained brain sections from a sham-lesioned mouse (**B**) and a DTg lesioned mouse (**C**). **D**. Reconstructions of DTg lesions (solid outlines) ordered from caudal (top) to rostral (down) DTg (Franklin and Paxinos, 2008). Each color represents one mouse case. Distance from bregma is indicated in mm (Franklin and Paxinos, 2008). (For interpretation of the references to color in this figure legend, the reader is referred to the Web version of this article.)

significances calculated from these latter tests are represented on the figures. Non-parametric Spearman correlation coefficients were calculated for comparing the extent of DTg lesions to sleep and wake amounts.

For the data extracted from patch clamp electrophysiological recordings, Friedman tests were performed to compare mean firing frequencies from aCSF, 8-OH-DPAT and aCSF wash conditions, and from aCSF, WAY 100635 and WAY 100635 + 8-OH-DPAT co-perfusion conditions as described above, followed by Dunn's multiple comparisons tests. All data were expressed as mean ± S.E.M.

3. Results

3.1. 5-HT$_{1A}$R are expressed by GABAergic neurons in the DTg

We first used 5-HT$_{1A}$-iCre/R26R mice to precise further the localization of 5-HT$_{1A}$R-expressing cells that we previously identified in the DTg (Bonnavion et al., 2010, Fig. 1). In this transgenic line, the mouse 5-HT$_{1A}$R gene drives the expression of the Cre recombinase that, in turn, activates the expression of β-galactosidase (Sahly et al., 2007). Analysis of β-galactosidase activity, revealed by a specific blue labeling, showed that blue stained neurons expressing 5-HT$_{1A}$R are distributed preferentially in the ventral part of the DTg (Fig. 1A–B) extending from −5.1 to −5.4 mm relative to bregma. At this caudo-rostral level, some stained neurons are localized in the caudal part of the dorsal raphe nucleus (DRc, Fig. 1B). In control conditions, R26R heterozygous mouse brain sections showed no β-galactosidase staining (data not shown). Dual *ISH* experiments were then performed to identify the phenotype of 5-HT$_{1A}$R mRNA expressing neurons in the DTg. We found that GABAergic neurons labeled by the GAD67 riboprobe (pink labeling) span the entire DTg (Fig. 1C). Co-localization with 5-HT$_{1A}$R mRNA hybridization signal was mainly observed in the ventral part of the DTg, indicating the preferential location of 5-HT$_{1A}$R expressing GABAergic neurons in this DTg subarea (Fig. 1C).

3.2. Electrolytic lesion of the DTg promotes wake

To assess the possible implication of the DTg in sleep regulation, we first examined the consequences of DTg lesions on sleep and

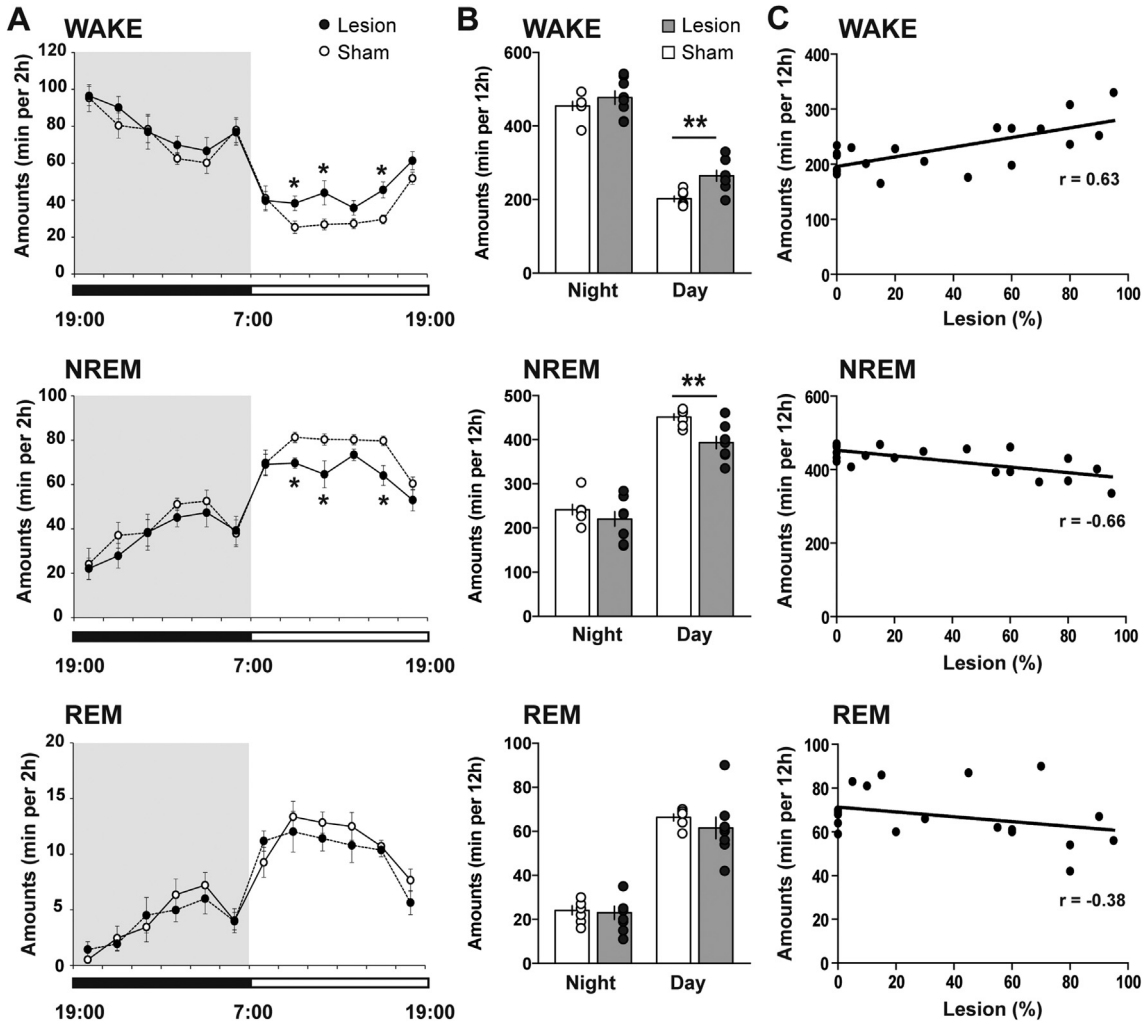

Fig. 3. The effects of DTg bilateral lesion on sleep-wake patterns. **A**. Sleep-wake states across the light/dark cycle in sham-lesioned (open circles, N = 7) and lesioned (black filled circles, N = 8) mice. The data are expressed as minutes per 2 h for the amounts of vigilance states. **B**. Amounts of wake, NREM sleep and REM sleep expressed as minutes per 12 h during both the night and the light period in sham-lesioned (open bars, N = 7) and lesioned (black filled bars, N = 8)) mice. **C**. The extent (%) of the lesion correlates significantly with the amount of wake (top, $^{**}P < 0.01$), NREM sleep (middle, $^{**}P < 0.01$), but not REM sleep (bottom, $P = 0.09$) during the light period (N = 21). All data are expressed as means ± S.E.M. Mann Whitney tests were applied to assess the differences between sham and lesioned mice ($^{*}P < 0.05$). Spearman correlation tests were performed between the amounts (ordinate) of each vigilance state and the extent of lesion (abscissa).

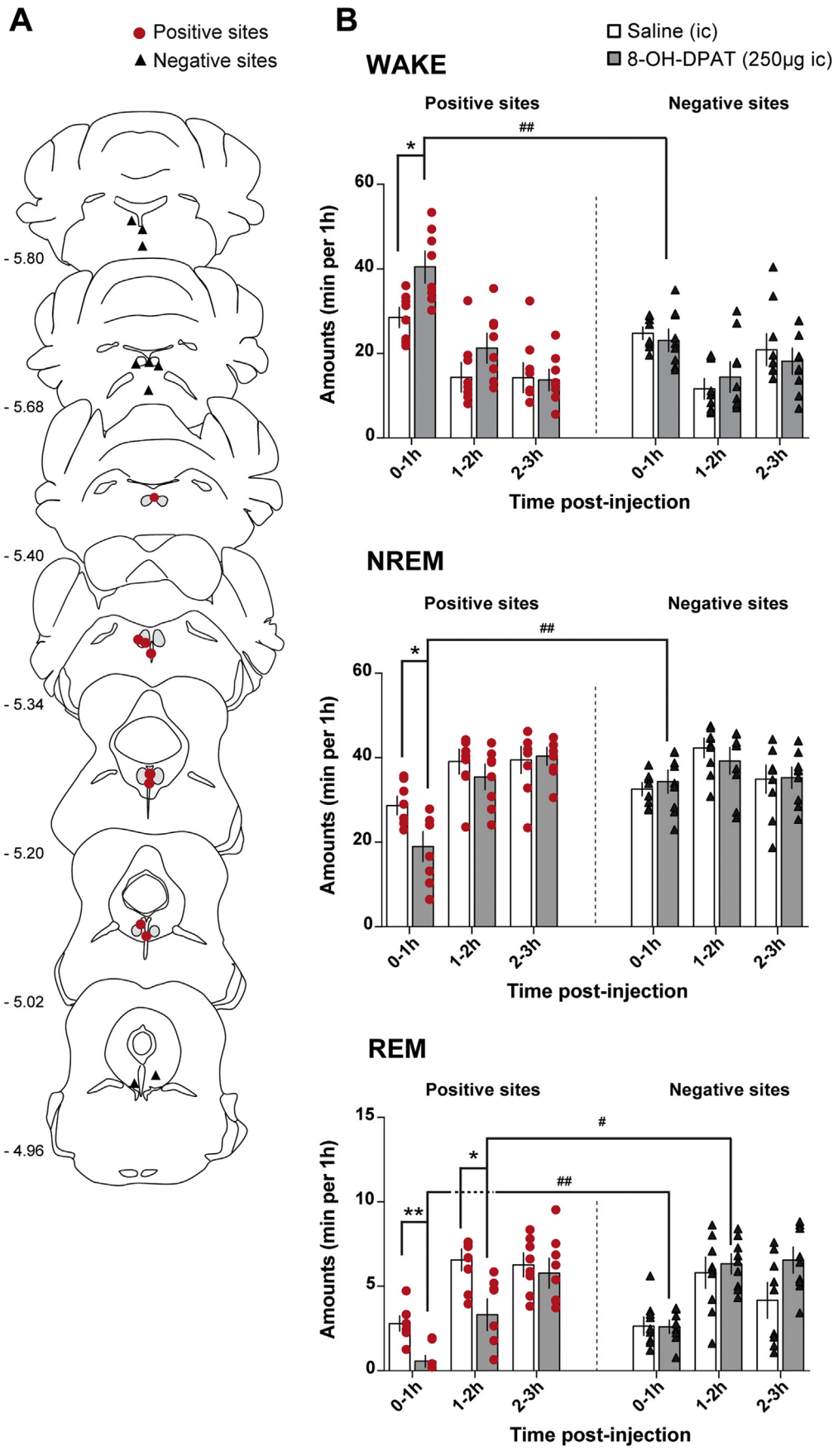
A
Positive sites
Negative sites
- 5.80
- 5.68
- 5.40
- 5.34
- 5.20
- 5.02
- 4.96
B
Saline (ic)
8-OH-DPAT (250µg ic)
WAKE
Positive sites
Negative sites
Amounts (min per 1h)
Time post-injection
0-1h
1-2h
2-3h
NREM
REM

wakefulness. Small intensity currents were delivered to make bilateral lesions of the DTg in 14 mice. A representative example of bilateral lesions is shown after Nissl (Fig. 2A–C) and NeuN (Supplementary Fig. 1) staining. In six of these mice, DTg lesion was partial, with only 21 ± 7% of the nucleus destroyed, but in the remaining 8 mice, extended lesion was achieved with an average of 74 ± 6%. In three cases, the bilateral lesions extended to the midline including the more caudal part of the DRc. For each mouse, the extent of the lesion is illustrated in Fig. 2D. For these experiments, the control group (N = 7) corresponded to sham-lesioned mice.

Mice with extended lesions (N = 8) showed an increase in wake amounts (+31%; $^{**}P = 0.002$; Fig. 3A–B) at the expense of NREM sleep (−13%; $^{**}P = 0.003$; Fig. 3A–B) compared with sham-lesioned mice (N = 7) during the light period, but not during the dark active period. As a result, the whole-day enhancement of wake amounts in lesioned mice compared with sham-lesioned mice reached only +13% (data not shown). The limited amplitude of these changes in wake amounts explains why they were not associated with any significant modifications of the number of wake episodes or bout mean duration (Supplementary Table 3). On the other hand, lesions of the DTg did not significantly affect REM sleep amounts despite a trend toward reduction ($P = 0.08$; Fig. 3A–B). To evaluate whether the extent of lesion correlated with the increase in wake, a regression analysis including all lesioned mice (N = 14) was performed (Fig. 3C). A strong positive correlation was observed between the extent of the lesion and wake amounts during the light period (r = 0.63; $^{**}P = 0.002$). Conversely, NREM sleep amounts negatively correlated with the extent of the lesion (r = 0.66; $^{**}P = 0.001$). Finally, no correlation was found between DTg lesion and REM sleep amounts during the light period (r = 0.38; $P = 0.09$).

Hence, these results showed that DTg lesions promoted wake during the "resting" light period suggesting that DTg neurons might be part of the network that modulates sleep-wake stages.

3.3. 5-HT$_{1A}$R in the DTg modulate vigilance states

We next investigated the effect of microinjections of the 5-HT$_{1A}$R agonist 8-OH-DPAT into the DTg on vigilance states. Polysomnographic recordings were made in freely moving mice after microinjection (ZT 3) of 8-OH-DPAT (250 pg, 50 nl) or saline (50 nl, control) into the DTg (Fig. 4). On completion of the recordings, histological inspection of the microinjection sites was performed after local injection of pontamine sky blue dye. This allowed us to distinguish two groups of mice (Fig. 4A) independently of the sleep results. Injection sites within or at a distance of less than 200 μm from the center of the DTg (at bregma −5.25 mm as defined by our anatomical characterization of this nucleus in the Materials and Methods) were considered as "positive" sites (N = 8; Fig. 4A). A typical example of the pontamine sky blue staining obtained in a "positive" mouse is illustrated in Supplementary Fig. 2A. "Negative" sites corresponded to injection sites located at further rostro-caudal levels and were considered as controls for locus specificity (N = 9). The consequences of 8-OH-DPAT microinjections on vigilance states were then analyzed in the two groups. In addition, to control the injection target of 8-OH-DPAT within the DTg, we examined in two mice the labeling of [^{3}H]8-OH-DPAT microinjected locally. We found that it covered bilaterally the entire DTg, but also included the more caudal part of the DR (Supplementary Fig. 3).

Microinjection of 8-OH-DPAT into "positive" sites within the DTg disrupted sleep-wake pattern while it had no effect on sleep architecture when performed into "negative" sites (Fig. 4B). In "positive" sites, 8-OH-DPAT increased wake amounts during the first hour post-injection compared with saline microinjection (+42%; $^{*}P = 0.016$, Fig. 4B WAKE). In parallel, NREM sleep (−34%; $^{*}P = 0.016$, Fig. 4B NREM) and especially REM sleep (−80%; $^{**}P = 0.008$, Fig. 4B REM) amounts were reduced. For the next two following hours, wake (1–2 h: $P = 0.25$; and 2–3 h: $P = 0.87$) and NREM sleep (1–2 h: $P = 0.25$; and 2–3 h: $P > 0.99$) amounts in 8-OH-DPAT-microinjected mice returned to levels not significantly different from those recorded in saline-injected controls. However, the effects of 8-OH-DPAT on the cumulative total amounts of time of wake and NREM sleep over the first 2 h remained significant (0–2 h: $^{*}P < 0.05$; Supplementary Table 2). These effects were more robust on the reduction of REM sleep amounts, which significantly persisted during the second hour post 8-OH-DPAT injection (1–2 h: $^{*}P = 0.016$; 0–2 h: $^{***}P < 0.001$; Supplementary Table 2). This REM sleep inhibition induced by 8-OH-DPAT microinjection into the "positive" sites resulted from a reduction in the number of REM sleep bouts (Supplementary Table 3) and an increased latency for the first REM sleep episode to occur after treatment (23.6 ± 3.9 min and 66.4 ± 13.4 min after intra-DTg microinjection of saline and 8-OH-DPAT, respectively, Ratio paired t-test, $^{**}P = 0.004$; 26.4 ± 2.1 min and 66.4 ± 13.4 min in mice injected with 8-OH-DPAT into "negative" and "positive" sites, respectively, Unpaired t-test with Welch's correction, $^{*}P = 0.02$). REM sleep amounts subsequently returned to the control values observed with saline injection during the third hour after 8-OH-DPAT microinjection into "positive" sites ($P = 0.71$). A representative example of such modifications is illustrated in the Supplementary Fig. 2B.

In contrast to the alterations in sleep-wake pattern in mice injected into the "positive" sites, no significant changes in wake ($P = 0.65$), NREM sleep ($P = 0.23$) and REM sleep ($P = 0.59$) were observed in mice injected with 8-OH-DPAT into the "negative" sites (Fig. 4B), located more than 200 μm apart from DTg center. Altogether, our data suggest that the activation of 5-HT$_{1A}$R in the DTg had a wake promoting influence at the expense of both NREM and REM sleep, and strongly inhibited REM sleep.

3.4. GABAergic DTg neurons are inhibited by the activation of 5-HT$_{1A}$R

As 8-OH-DPAT displays affinity for both 5-HT$_{1A}$R and 5-HT$_7$R, we further assessed *ex vivo* the specific involvement of 5-HT$_{1A}$R. We performed patch-clamp recordings of DTg neurons in loose-seal configuration for minimal perturbation of their homeostasis in response to 5-HT$_{1A}$R agonist and antagonist (Fig. 5). Recorded neurons confined to the DTg (Fig. 5A) showed spontaneous

Fig. 4. Activation of 5-HT$_{1A}$R in the DTg enhances wake and reduces REM sleep. **A**. Schematic drawings showing 8-OH-DPAT microinjection sites. Positive (n = 8, red dots) and negative (n = 9, black triangles) injection sites were dyed with pontamine sky blue and reported in atlas plates at seven different levels of the brainstem (Franklin and Paxinos, 2008). Injection sites within or adjacent to the DTg are considered as positive sites. Negative sites are localized, at least, 200 μm apart from the center of the DTg. The grey area corresponds to the DTg nucleus. Each symbol represents the injection site in one mouse. Distance from bregma is indicated in mm (from Franklin and Paxinos, 2008). **B**. Consequences of 8-OH-DPAT microinjections into the DTg on wake, NREM and REM sleep. Bars represent the amounts of the different vigilance states expressed as minutes per 1 h during the first 3 h of the recording period (N = 8 "positive sites", red circles; N = 9 "negative sites", black triangles) after saline (open bars) and 8-OH-DPAT (grey filled bars) injections. Two-way repeated measures (RM) ANOVA between pharmacological conditions and locus groups showed a significant interaction for each vigilance state on the first hour of recording at the exception of REM sleep, where interaction is significantly different for the first 2 h of recordings (WAKE: $^{***}P < 0.001$, F(1,15) = 18.23; NREM sleep: $^{**}P < 0.01$, F(1,15) = 13.87; REM sleep 0–1 h: $^{*}P < 0.05$ F(1,15) = 6.94 and REM sleep 1–2 h:$^{*}P < 0.05$ F(1,15) = 7.43). These ANOVA were followed by Wilcoxon tests between drug conditions ($^{*}P < 0.05$, $^{**}P < 0.01$) and Mann-Whitney tests between locus groups ($^{\#}P < 0.05$, $^{\#\#}P < 0.01$). Data are expressed as means ± S.E.M. (For interpretation of the references to color in this figure legend, the reader is referred to the Web version of this article.)

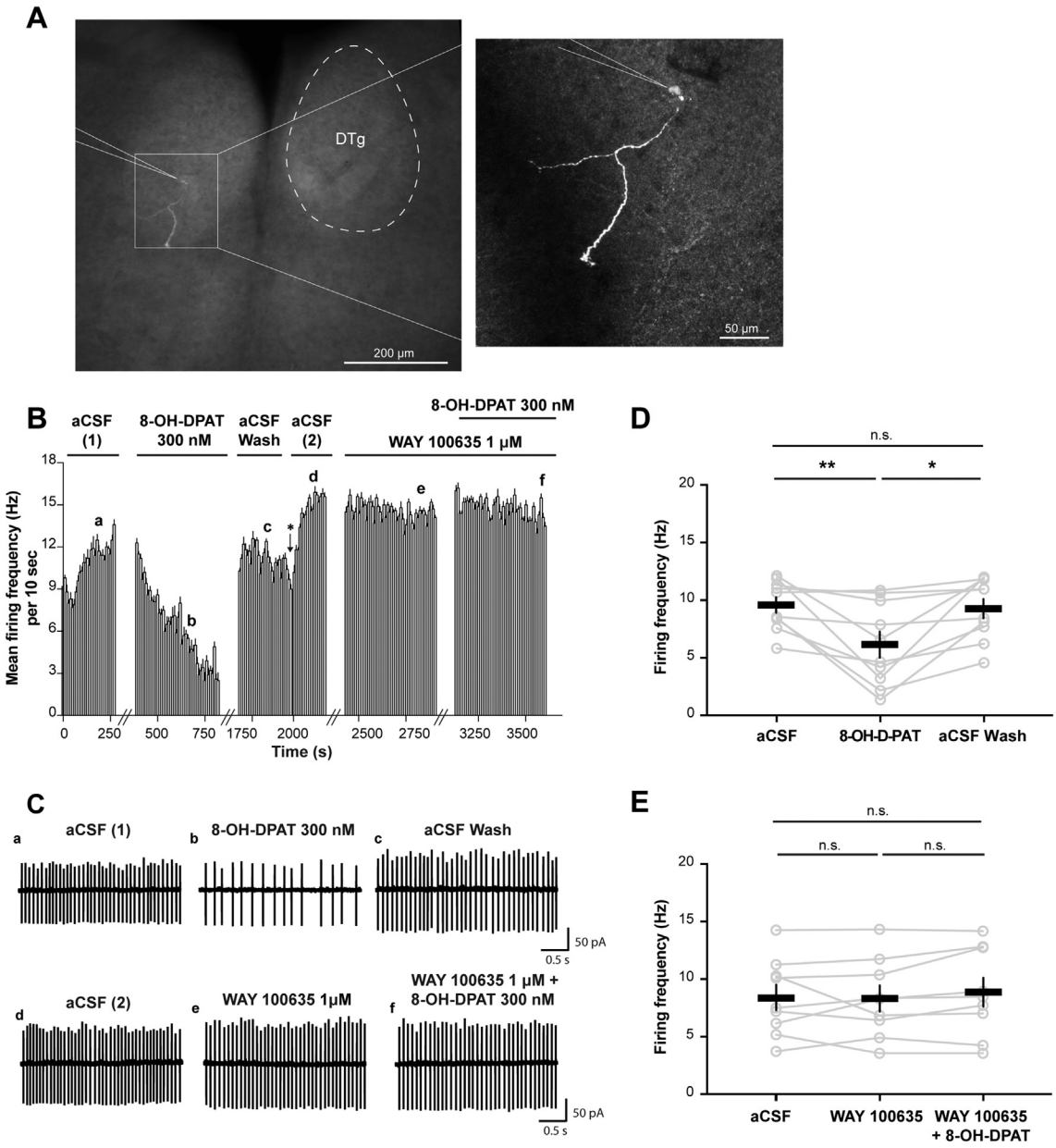

Fig. 5. Inhibitory effects of 8-OH-DPAT on DTg neurons in a loose-seal patch configuration. A. Localization of a recorded neuron in the DTg. Left: Photomicrograph showing a typical mouse DTg slice containing one patched neuron filled with biocytin (0.5%), revealed with streptavidin-NL557 nm. Right: Magnification of the framed region showing the patched neuron. **B**. Mean firing rates from a recording of a responding DTg neuron: **a**) during aCSF baseline, **b**) during the 8-OH-DPAT perfusion (300 nM), **c**) at the end of the aCSF wash, **d**) during aCSF second baseline, **e**) during perfusion of the selective 5-HT_{1A} antagonist, WAY 100635 (1 µM), and **f**) during the co-perfusion with 8-OH-DPAT (300 nM). Each histogram bar represents mean firing rate calculated over 10-s bin interval ± S.E.M. The arrow and asterisk represent the re-positioning of the micropipette to maintain a proper loose-seal leading to a mechanical excitation of the cell (aCSF baseline 2 in **d**). **C**. Extracellular action potentials taken from position **a-f** in **B**. **D-E**. Population graph summaries showing: (**D**) the inhibitory effects of bath-applied 8-OH-DPAT (300 nM) on the firing rate of DTg neurons (N = 10), and (**E**) selective prevention of 8-OH-DPAT mediated response by WAY 100635 (1 µM) in another set of DTg neurons (N = 9). Grey circles connected by lines represent values for individual neurons. Group means ± S.E.M are represented by the black lines for each condition. Non-parametric ANOVA Friedman tests were performed (**D**: $^{**}P < 0.01$, **E**: $P = 0.28$) followed by Dunn's multiple comparisons tests illustrated in the graphs: $^{**}P < 0.01$, $^{*}P < 0.05$, n.s. not significant $P > 0.05$.

discharge activity with a mean firing frequency of 8.7 ± 0.6 Hz (N = 23) during baseline aCSF recordings. In another series of patch-clamp recordings, we recorded DTg neurons in whole-cell configuration to extract their passive and active membrane properties (see Supplementary Fig. 4).

We tested the effects of 8-OH-DPAT (300 nM) on 14 neurons. We found that 10/14 neurons were progressively inhibited by 8-OH-DPAT (Fig. 5B–D) resulting in a significant decrease in their mean firing frequency (Friedman test $^{**}P < 0.01$) from 9.6 ± 0.7 Hz at aCSF baseline (taken over 2 min before 5-HT_{1A} agonist application), to 6.1 ± 1.1 Hz at their maximal response to 8-OH-DPAT ($^{**}P < 0.01$). As shown in Fig. 5B–C(a,b,c) and Fig. 5E, this action of 8-OH-DPAT was fully reversed by aCSF washout ($^{*}P < 0.05$), with the firing rate back to a value (9.3 ± 0.8 Hz) not significantly different from baseline ($P > 0.99$). These neurons were individually selected based on a significant variation greater than baseline mean firing frequency ± 2× S.E.M. in response to 8-OH-DPAT. The spontaneous firing activity of the four remaining neurons was not significantly affected by 8-OH-DPAT application (Friedman test $P = 0.43$; aCSF baseline: 7.9 ± 2 Hz, 8-OH-DPAT: 8.1 ± 2.1 Hz, aCSF wash: 7.5 ± 1.4 Hz). Thus,

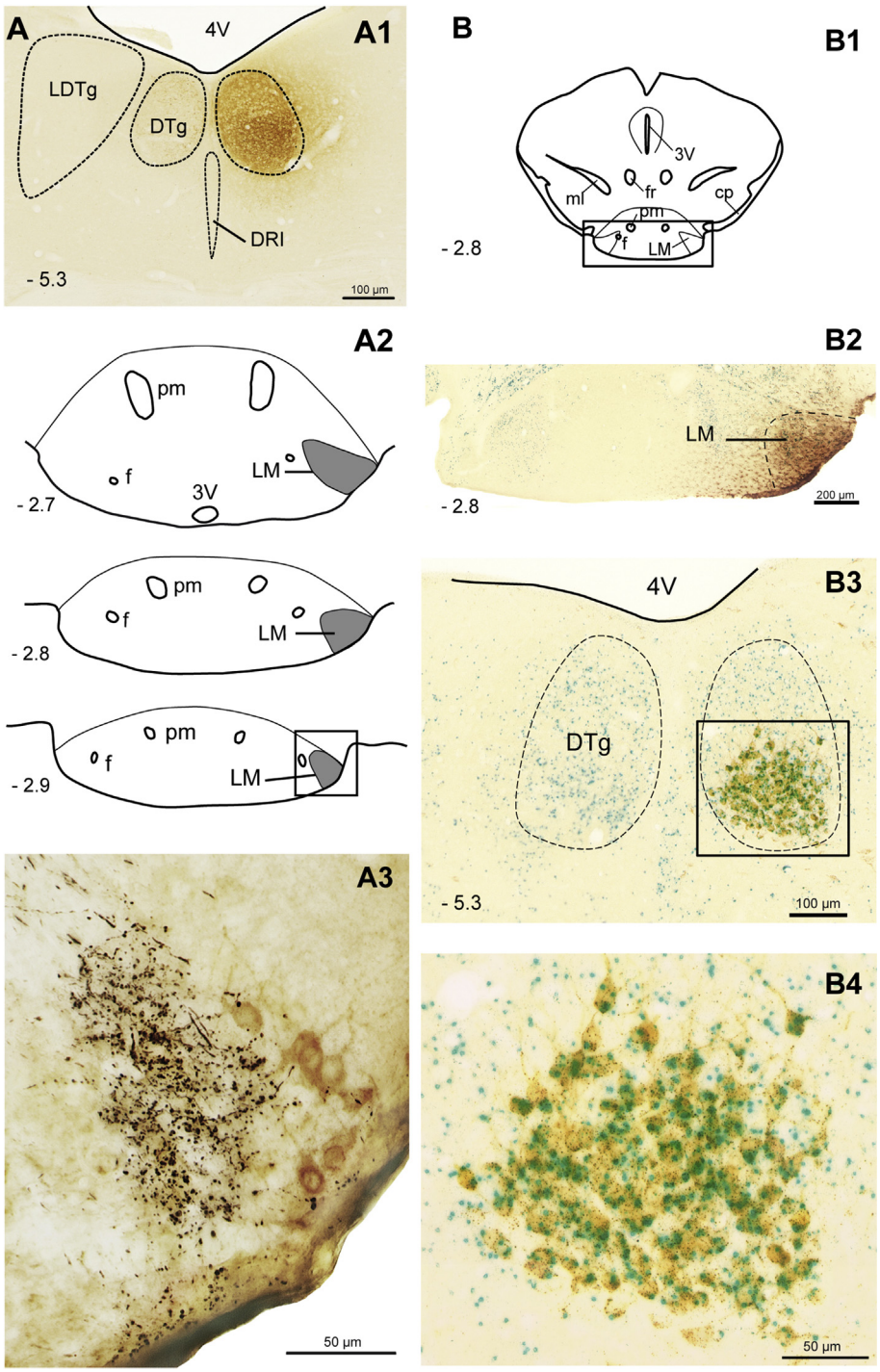

Fig. 6. 5-HT_{1A}R expressing neurons of the DTg mainly target non histaminergic neurons in the LM. **A.** Anterograde tracing from the DTg. **A1**. Photomicrograph of PHA-L injection site (brown staining) located in the DTg. **A2**. Drawings illustrating the extent of PHA-L labeled axons and terminals innervating the LM. This series of coronal section drawings correspond roughly, from caudal to rostral, to Bregma levels −2.9 to −2.7 mm (Franklin and Paxinos, 2008). The framed region corresponds to the photomicrograph in **A3**. **A3.** Photomicrograph showing PHA-L labeled axons and terminal boutons originating from the DTg (black staining) and histaminergic neurons immunostained for histidine decarboxylase (brown cytoplasmic neurons) in the LM. **B**. Retrograde tracing from the LM. **B1**. Coronal section at the level of the LM adapted from the stereotaxic atlas of Franklin and Paxinos (2008). The framed region in **B1** corresponds to the photomicrograph in **B2**. **B2**. Photomicrograph of Fluorogold injection site (brown staining) located in the LM. **B3**. Retrogradely labeled neurons (brown staining) were seen in the ventral part of the DTg. The framed region in **B3** corresponds to the photomicrograph in **B4**. **B4**. Photomicrograph of 5-HT_{1A}R expressing neurons (blue staining) retrolabeled for Fluorogold (brown staining) in the ventral part of the DTg. Distance from bregma is indicated in mm (Franklin and Paxinos, 2008). (For interpretation of the references to color in this figure legend, the reader is referred to the Web version of this article.)

the majority of DTg neurons recorded (71%) was found to be inhibited by 8-OH-DPAT.

To further confirm the selective involvement of 5-HT_{1A}R, we pre-applied WAY 100635 followed by WAY 100635 (1 µM) + 8-OH-DPAT (300 nM) co-perfusion on DTg slices (Fig. 5B–C, E). On 9/9 neurons, the pre-application of WAY 100635 (1 µM) prevented the 8-OH-DPAT inhibition of firing without modifying the group baseline mean firing rate (Friedman test $P = 0.28$; aCSF baseline:

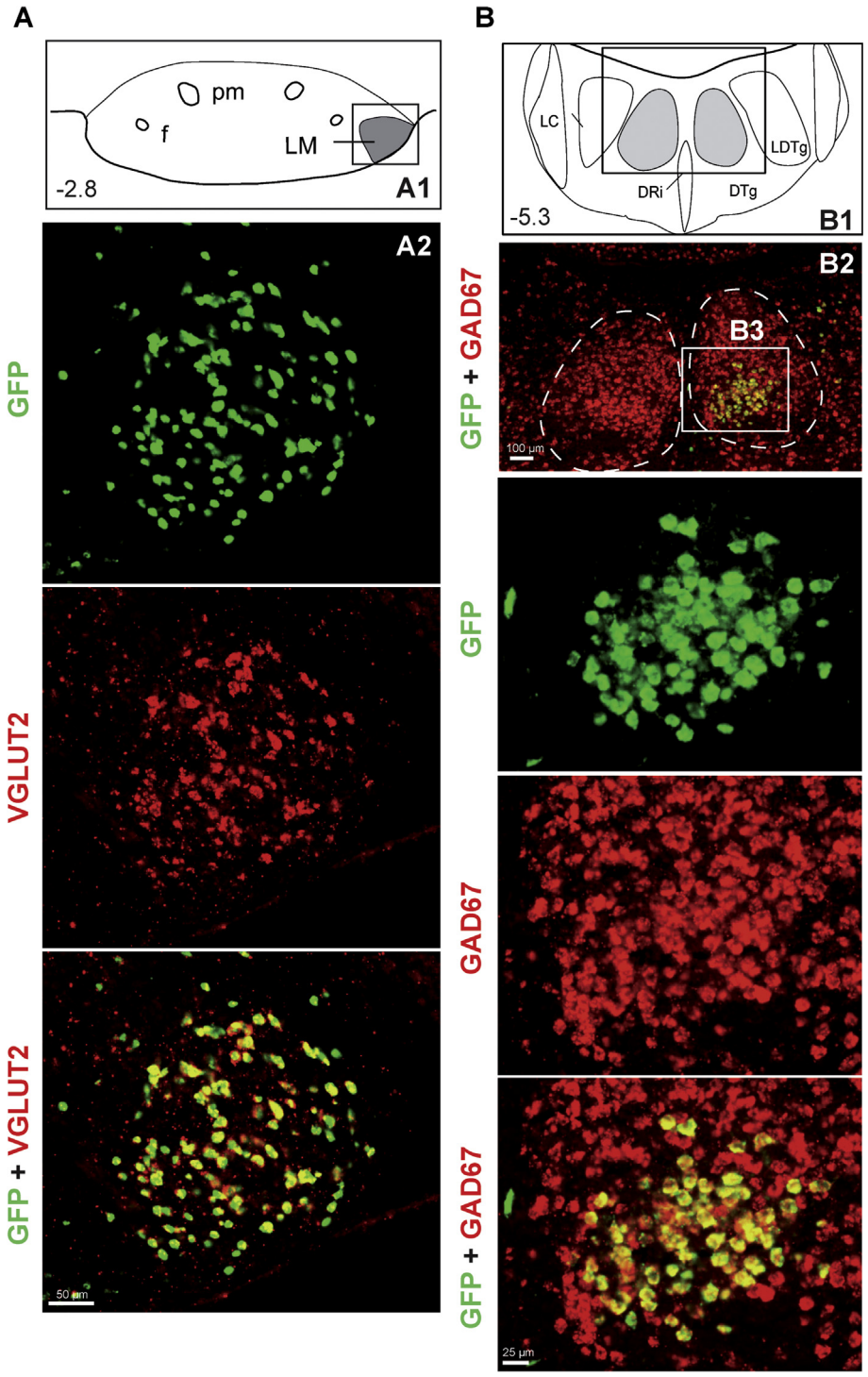

Fig. 7. Synaptic inputs to glutamatergic (VGLUT2) neurons in the LM using cell-type specific rabies virus-based monosynaptic tracing in VGLUT2-ires-cre mice. **A.** Identification of the infected neurons in the LM of VGLUT2-ires-cre mice. **A1:** Coronal view at the level of the LM (grey area) adapted from the stereotaxic atlas of Franklin and Paxinos (2008). **A2.** Selective expression of GFP mRNA (green) corresponding to infected cells (top), and of VGLUT2 mRNA (red) corresponding to glutamatergic neurons (middle). The merged image (bottom) shows selective expression of GFP in glutamate VGLUT2 neurons of the LM (yellow, expressing both GFP and VGLUT2). **B.** Identification of the retrogradely labeled neurons in the DTg. **B1:** Coronal view at the level of the DTg (grey area) adapted from the stereotaxic atlas of Franklin and Paxinos (2008). **B2.** High magnification superimposed image of GFP (green) and GAD67 (red) mRNA expression in the DTg area after monosynaptic viral tracing in VGLUT2-ires-cre mice. Yellow cells correspond to neurons expressing both GFP and GAD67 mRNAs. **B3.** Magnification of the framed region in B2 showing selective expression of GFP (green) corresponding to retrogradely labeled neurons (top), and of GAD67 (red) corresponding to GABAergic neurons (middle). The merged image (bottom) shows selective expression of GFP in GABAergic neurons of the ventral part of the DTg (yellow, expressing both GFP and GAD67). Distance from bregma is indicated in mm (Franklin and Paxinos, 2008). (For interpretation of the references to color in this figure legend, the reader is referred to the Web version of this article.)

8.4 ± 1.1 Hz, WAY 100635: 8.3 ± 1.1 Hz; WAY 100635 + 8-OH-DPAT: 8.8 ± 1.2 Hz; Fig. 5B–C(d,e,f), E). However, looking at individual responses, we noticed that the application of WAY 100635 in two cells increased firing rate from baseline values (N = 2/9). In one cell the opposite effect of WAY 100635 application was observed (N = 1/9), whereas the firing activity of the majority of recorded DTg neurons remains unaffected by WAY 100635 application (N = 6/9). These individual responses indicate that certain DTg cells exhibit some variability in their firing rate and/or there may be an endogenous 5-HT tone on which WAY 100635 had an effect. However, collectively, these *ex vivo* recordings showed that the agonist 8-OH-PAT inhibits the activity of DTg neurons by specifically acting on 5-HT_{1A}R.

3.5. GABAergic DTg neurons exclusively target glutamatergic neurons of the caudal hypothalamus

To identify the anatomical targets of DTg neurons, anterograde tracing experiments were performed in C57Bl/6J mice (Fig. 6A). PHA-L tracer was injected into the DTg (Fig. 6A1). Similarly to what had been found in other mammal species (Hayakawa and Zyo, 1984), a dense terminal labeling appeared ipsilaterally in the lateral mammillary nucleus (LM) of the mammillary bodies throughout its caudo-rostral extension in the mouse brain (Fig. 6A2). The rest of the brain was completely devoid of PHA-L labeling showing that DTg neurons project exclusively to the LM. Because histaminergic neurons of the tuberomammillary nucleus (TMN), which forms a shell around the ventral parts of the mammillary bodies (Panula et al., 1984), are known to play a key role in wake maintenance (Takahashi et al., 2006), we examined whether neurons of the DTg could directly contact them. Double immunostaining was then performed to visualize PHA-L immunoreactive fibers and HDC immunoreactive cell bodies. As shown in Fig. 6A3, PHA-L labeled terminals from the DTg were seen in close proximity to HDC immunoreactive histaminergic neurons. However, appositions between PHA-L labeled fibers and HDC-immunolabeled neurons were only rarely visualized, indicating that DTg neurons target mainly neurons of an unknown phenotype in close proximity to histaminergic neurons.

Projection from the DTg to the LM was further confirmed by using the Fluorogold retrograde tracer injected into the LM of 5-HT_{1A}-iCre/R26R mice (Fig. 6B). In these mice, all the cells that have an active promoter of the 5-HT_{1A}R gene can be visualized with a highly sensitive X-Gal staining (Sahly et al., 2007). A Fluorogold injection targeting the LM is shown in Fig. 6B1-B2. A large number of retrogradely labeled neurons was found ipsilaterally in the ventral part of the DTg (Fig. 6B3-B4). They nearly all expressed the 5-HT_{1A}R as evidenced by blue dots present in the cytoplasm of Fluorogold immunoreactive neurons stained in brown (Fig. 6B4).

In addition to histaminergic neurons, the LM contains a high number of VGLUT2-positive neurons as revealed by FISH labeling (Fig. 7A). We next asked whether LM glutamatergic (VGLUT2) neurons may be a critical target for DTg GABAergic neurons. To test this hypothesis, we mapped inputs to VGLUT2 neurons of the LM using monosynaptic rabies tracing (Kohara et al., 2014). Rabies virus and cre-dependent helper AAV were microinjected into the LM of VGLUT2-ires-cre mice to selectively target VGLUT2 neurons. To examine the cell-type-specificity of the infected neurons and the phenotype of retrogradely labeled neurons, we performed mRNA-selective dual FISH. Probes towards VGLUT2 and GFP mRNAs were included for detection of the infected neurons in the LM (Fig. 7A), and GAD67 and GFP mRNAs for detection of retrogradelly labeled neurons in the DTg (Fig. 7B). Dual FISH in the LM showed that all GFP positive neurons express VGLUT2 mRNA confirming that all infected neurons are glutamatergic VGLUT2 neurons (Fig. 7A2). As shown in Fig. 7B, retrogradely labeled neurons as revealed by GFP expression are exclusively found in the ventral part of the DTg. Importantly, these neurons are GABAergic as shown by the perfect co-localization of GFP and GAD67 mRNA labeling (Fig. 7B2-3). This retrograde mapping showed that LM glutamatergic VGLUT2 neurons receive direct inputs from GABAergic neurons of the ventral DTg.

Altogether, this anatomical study revealed that 5-HT_{1A}R expressing GABAergic neurons in the ventral DTg exclusively target glutamatergicVGLUT2, but not histaminergic, neurons in the LM.

4. Discussion

In this study, we show that the DTg, a brainstem GABAergic nucleus expressing high levels of 5-HT_{1A}R, is involved in the regulation of wakefulness. Previous electrophysiological, pharmacological and genetic studies had evidenced a role for 5-HT neurons in promoting wake and inhibiting REM sleep (McGinty and Harper, 1976; Rasmussen et al., 1984; Sakai, 2011). Although numerous reports had addressed the possibility that 5-HT_{1A}R could mediate the influence of 5-HT on sleep, the specific structures where they would play such a role had not been identified. Here, we show that one of these structures is the DTg. Indeed, lesion of the DTg promotes wake and microinjection of the prototypical 5-HT_{1A}R agonist 8-OH-DPAT into this nucleus promotes wake and inhibits REM sleep. Finally, we identify glutamatergic neurons of the hypothalamic LM as the exclusive target of DTg neurons. Overall, these results suggest that 5-HT promotes wake by exerting an inhibitory control mediated by 5-HT_{1A}R on GABAergic DTg neurons projecting to the LM.

4.1. The DTg as a key structure in 5-HT-mediated wake/sleep regulation

The principal goal of our study was to assess the influence of the DTg on vigilance states in connection with the 5-HT system. We had previously identified this nucleus as being essentially GABAergic (Bonnavion et al., 2010). We now report that local activation of the 5-HT_{1A}R in this nucleus enhances wake and reduces REM sleep, which mimics the effects observed after the systemic administration of the agonist 8-OH-DPAT (Portas and Grønli, 2008). The wake-promoting effects are also recapitulated by DTg lesions. However, REM sleep inhibition is only observed after acute pharmacological inactivation of the DTg and not after its lesion. Such discrepancy might be accounted for by compensatory mechanisms triggered by the lesion, as sleep was recorded at least 2 weeks away from the lesionning procedure.

Besides, because the DTg is composed of extremely small bilateral nuclei, lesions or 8-OH-DPAT microinjections might have impacted adjacent regions. Indeed, the agonist could spread away from the injection site (see Supplementary Fig. 2) and thus reach the caudal part of the dorsal raphe nucleus (DRN) that comprises somatodendritic 5-HT_{1A} autoreceptors on 5-HT neurons. While we cannot rule out a possible involvement of the latter nucleus in our sleep analysis convergent data are not in support of the implication of somatodendritic 5-HT_{1A} autoreceptors on 5-HT neurons in the DR but rather favor the idea of the specific involvement of 5-HT_{1A}R on DTg neurons. In particular, 1) injections of 8-OH-DPAT caudally or rostrally to the DTg (more than 200 μm apart from the nucleus) had no effect on wake/sleep parameters (Fig. 2) and 2) activation of 5-HT_{1A} autoreceptors in the DRN results in an increase (Portas et al., 1996; Bjorvatn et al., 1997) or no change (Sakai and Crochet, 2001) of REM sleep, and 3) large lesions of the 5-HT cells in the DR do not modify the sleep/wake cycle in rats (Tissier et al., 1993). Therefore, it can be reasonably concluded that the 5-HT_{1A}R within the DTg

actually mediate the 8-OH-DPAT-induced wake enhancement and REM sleep inhibition. Overall, both the electrolytic lesion of the DTg and its pharmacological inactivation (through inhibitory 5-HT_{1A}R) produced a common effect, i.e. wake promotion, thus validating further the involvement of the DTg in sleep/wake regulation.

As 8-OH-DPAT acts on both 5-HT_{1A}R and 5-HT_7R, we therefore addressed the specific involvement of 5-HT_{1A}R *ex vivo* on brain slices including the DTg. We found that the vast majority of DTg neurons were inhibited by 8-OH-DPAT, an effect that was prevented by the application of the selective 5-HT_{1A}R antagonist, WAY 100635. Additionally, we investigated the presence of 5-HT_7R in the DTg using dual FISH, and found that 5-HT_7R expressing neurons are barely present in the mouse DTg in comparison to LDTg/parabrachial region (Supplementary Fig. 5). Altogether, these results brought further evidences that 5-HT exerts an inhibitory control over GABAergic neurons of the DTg impacting sleep/wake states.

4.2. The ACh-5-HT hypothesis of sleep-wake regulation revisited

Up to now, 5-HT inhibition of REM sleep was proposed to rely on a reciprocal inhibition between REM sleep active (REM-on) cholinergic neurons of the pedunculopontine and laterodorsal tegmentum (PPTg/LDTg) nuclei on the one hand, and monoaminergic REM sleep inactive (REM-off) neurons on the other hand (Hobson et al., 1975). Support to this theory notably includes *in vitro* and *in vivo* electrophysiological data showing that 5-HT inhibits the activity of cholinergic LDTg/PPTg neurons *via* 5-HT_{1A}R activation in rats (Luebke et al., 1992), cats (Thakkar et al., 1998) and guinea pigs (Leonard and Llinás, 1994). However, local microinjection of 5-HT_{1A}R agonists into the LDTg/PPTg was reported to either inhibit REM sleep without affecting wake (Horner et al., 1997; Monti and Jantos, 2003) or exert no effect on sleep (Sanford et al., 1996; Datta et al., 2003; Grace et al., 2012). These contradictory findings have been attributed to anatomical differences between species, to the specificity of different ligands used or to age differences. However, none of these studies controlled for the ligand diffusion, defined the anatomical region involved, or investigated for the presence of 5-HT_{1A}R in the LDTg/PPTg nuclei. In light of our present data, these points might be critical issues because the DTg, which contains high density of 5-HT_{1A}R, lies just next to the LDTg and thus could have been the actual target for 8-OH-DPAT to trigger its effects on sleep. In addition, we demonstrated previously that 5-HT_{1A}R are not expressed by cholinergic neurons in the LDTg (Bonnavion et al., 2010). Altogether, our data would support the idea that the GABAergic neurons of the DTg, but not the cholinergic ones in the LDTg/PPTg, mediate 5-HT facilitation of wake. This inference is in line with recent reports asserting the role of GABAergic neurons in the brainstem and in the medulla in sleep/wake regulations (Boissard et al., 2003; Lu et al., 2006; Anaclet et al., 2014; Hayashi et al., 2015; Weber et al., 2015; Cox et al., 2016). Accordingly, we propose that GABAergic DTg neurons, which are under an inhibitory control driven by 5-HT wake-on neurons, participate to sleep/wake regulatory loops (Supplementary Fig. 6).

4.3. A new role for the Gudden's nucleus?

To date, the sole known function attributed to the DTg is to generate the head direction cell (HD) signal (Sharp et al., 2001; Bassett et al., 2007). HD cells encode the animal's head direction in the horizontal plane and are thus critical for navigation (see Taube, 2007 for review). They are mainly found within serially connected structures belonging to the Papez's circuit including the LM, the anterior dorsal thalamic nucleus, the postsubiculum, the retrosplenial cortex and the medial enthorhinal cortex. Actually, DTg neurons have reciprocal connections with the LM (Supplementary Fig. 6), a finding that is remarkably conserved across mammalian species (Hayakawa and Zyo, 1984; Shibata, 1987; Wirtshafter and Stratford, 1993; Saunders et al., 2012). Our results from both anterograde and retrograde tracing further show that neurons of the ventral part of the DTg exclusively innervate the glutamatergic cells of the LM in the mouse brain. Here, we propose an additional role for the DTg→LM pathway in sleep-wake behavior, in line with a recent report showing that neuronal activity in the HD system is closely dependent on sleep-wake states (Peyrache et al., 2015). Nevertheless, further studies will be necessary to determine whether DTg neurons exhibit a state-related activity pattern to strengthen its role in regulating sleep/wake stages.

The existence of a functional connection between the 5-HT system and the DTg is strongly supported by anatomical findings. Thus, the DTg contains a remarkably dense 5-HT terminal innervation issued from the median raphe nucleus (MRN; Bang et al., 2012; Muzerelle et al., 2016) and we found that virtually all DTg neurons projecting to the LM express 5-HT_{1A}R (Bonnavion et al., 2010). These findings allow us to describe a novel network through which 5-HT neurons can sustain wake. In this network, inhibition of GABAergic DTg neurons by 5-HT MRN neurons through Gi-coupled 5-HT_{1A}R activation would disinhibit glutamatergic LM neurons that, in turn, would facilitate wake occurrence (Supplementary Fig. 6). This model implies that glutamatergic LM neurons in the posterior hypothalamus can promote wake. Indeed the posterior hypothalamus, classically defined as a waking center (Sakai et al., 1990; Lin, 2000), contains wake-specific neurons that are active only during waking, evidenced by extracellular unit recordings in cats (Vanni-Mercier et al., 2003), rats (Steininger et al., 1999) and mice (Takahashi et al., 2006). Most of these wake-specific neurons have been identified by juxta-cellular labeling as histaminergic neurons in the TMN (Takahashi et al., 2006), adjacent to the LM. However, we found here that terminals from the DTg only rarely contact histaminergic neurons in the LM. Alternatively, non-histaminergic wake-active neurons have also been described in the posterior hypothalamus, within and surrounding the TMN/LM area (Vanni-Mercier et al., 2003; Takahashi et al., 2006), including glutamatergic cells (Pedersen et al., 2017), which therefore could be the target of GABAergic DTg neurons to modulate wakefulness.

Further investigations will be required to establish the causal role of the DTg and its connection with the LM in sleep-wake regulation. Here, our approaches including electrolytic lesions of the DTg have clear limitations due to the destruction of both somas and fibers of passage, which weaken the specific role we attributed to the DTg. These limitations can be overcome thanks to the use of chemo- or opto-genetic tools. Our findings by revealing that the glutamatergic LM is the exclusive target of the GABAergic DTg offer a unique opportunity for conditional expression of these engineered receptors through LM retrograde tracing.

5. Conclusion

This study provides the first evidence that the GABAergic DTg is a target for 5-HT regulation of sleep and wakefulness highlighting a new ponto-hypothalamic pathway through which 5-HT facilitates wakefulness (Supplementary Fig. 6). This pathway includes long-range projecting GABAergic neurons of the ventral part of the DTg that exclusively target glutamatergic neurons of the LM and receive inhibitory inputs from the MRN. We propose that 5-HT MRN neurons exert an inhibitory control on this DTg→LM pathway to modulate sleep-wake states bringing to light a new function of the DTg in the sleep-wake networks.

Funding and disclosure

This research was supported by Institut National de la Santé et de la Recherche Médicale, and Université Pierre et Marie Curie. During performance of this work, PB was supported by the Ministère de la Recherche et de la Technologie (MRT), the Fondation pour la Recherche Médicale and the European Marie Sklodowska-Curie Actions. The authors declare no conflict of interest.

Author's contributions

VF and PB equally contributed to this work. PB, JFB, MH, JA and VF designed and analyzed the studies. MC and PB performed and analyzed the electrophysiological patch clamp recordings. SD, AKE and PB performed and analyzed the monosynaptic tracing experiments. SD, JFB, PB and VF performed and analyzed all the anatomical studies. SD designed and validated the cRNA probes and FISH protocols. IS and FT provided the transgenic 5-HT_{1A}-iCre/R26R mice. All authors contributed to finalize the manuscript for submission for publication.

Acknowledgements

We dedicate this article to the memory of Dr. Jean-François Bernard, an exceptional scientist, wonderful supporter, and devoted friend. We would like to thank Pr. Karl-Klaus Conzelmann and Dr. Alexander Ghanem for their generous gift of the rabies virus, and Dr. Christophe Varin for valuable comments on the manuscript and analysis.

Appendix A. Supplementary data

Supplementary data related to this article can be found at https://doi.org/10.1016/j.neuropharm.2018.06.014.

References

Anaclet, C., Ferrari, L., Arrigoni, E., Bass, C.E., Saper, C.B., Lu, J., et al., 2014. The GABAergic parafacial zone is a medullary slow wave sleep-promoting center. Nat. Neurosci. 17 (9), 1217–1224.

Bang, S.J., Jensen, P., Dymecki, S.M., Commons, K.G., 2012. Projections and interconnections of genetically defined serotonin neurons in mice. Eur. J. Neurosci. 35 (1), 85–96.

Bassett, J.P., Tullman, M.L., Taube, J.S., 2007. Lesions of the tegmentomammillary circuit in the head direction system disrupt the head direction signal in the anterior thalamus. J. Neurosci. 27 (28), 7564–7577.

Bjorvatn, B., Fagerland, S., Eid, T., Ursin, R., 1997. Sleep/waking effects of a selective 5-HT_{1A} receptor agonist given systemically as well as perfused in the dorsal raphe nucleus in rats. Brain Res. 770 (1–2), 81–88.

Boissard, R., Fort, P., Gervasoni, D., Barbagli, B., Luppi, P.H., 2003. Localization of the GABAergic and non-GABAergic neurons projecting to the sublaterodorsal nucleus and potentially gating paradoxical sleep onset. Eur. J. Neurosci. 18 (6), 1627–1639.

Bonnavion, P., Bernard, J.F., Hamon, M., Adrien, J., Fabre, V., 2010. Heterogeneous distribution of the serotonin 5-HT(1A) receptor mRNA in chemically identified neurons of the mouse rostral brainstem: implications for the role of serotonin in the regulation of wakefulness and REM sleep. J. Comp. Neurol. 518 (14), 2744–2770.

Boutrel, B., Monaca, C., Hen, R., Hamon, M., Adrien, J., 2002. Involvement of 5-HT_{1A} receptors in homeostatic and stress-induced adaptive regulations of paradoxical sleep: studies in 5-HT_{1A} knock-out mice. J. Neurosci. 22 (11), 4686–4692.

Cox, J., Pinto, L., Dan, Y., 2016. Calcium imaging of sleep-wake related neuronal activity in the dorsal pons. Nat. Commun. 7, 10763.

Datta, S., Mavanji, V., Patterson, E.H., Ulloor, J., 2003. Regulation of rapid eye movement sleep in the freely moving rat: local microinjection of serotonin, norepinephrine, and adenosine into the brainstem. Sleep 26 (5), 513–520.

Dartsch, C., Chen, D., Persson, L., 1998. Multiple forms of rat stomach histidine decarboxylase may reflect posttranslational activation of the enzyme. Regul. Pept. 77 (1–3), 33–41.

Ericson, H., Watanabe, J., Köhler, C.H., 1987. Morphological analysis of the tuberomammillary nucleus in the rat brain: delineation of subgroups with antibody against l-histidine decarboxylase as a marker. J. Comp. Neurol. 263 (1), 1–24.

Franklin, K.B.J., Paxinos, G., 2008. The Mouse Brain in Stereotaxic Coordinates. Academic Press, San Diego.

Grace, K.P., Liu, H., Horner, R.L., 2012. 5-HT_{1A} receptor-responsive pedunculopontine tegmental neurons suppress REM sleep and respiratory motor activity. J. Neurosci. 32 (5), 1622–1633.

Hasegawa, E., Maejima, T., Yoshida, T., Masseck, O.A., Herlitze, S., Yoshioka, M., et al., 2017. Serotonin neurons in the dorsal raphe mediate the anticataplectic action of orexin neurons by reducing amygdala activity. Proc. Natl. Acad. Sci. U. S. A. 114 (17), E3526–E3535.

Hayakawa, T., Zyo, K., 1983. Comparative cytoarchitectonic study of Gudden's tegmental nuclei in some mammals. J. Comp. Neurol. 216 (3), 233–244.

Hayakawa, T., Zyo, K., 1984. Comparative anatomical study of the tegmentomammillary projections in some mammals: a horseradish peroxidase study. Brain Res. 300 (2), 335–349.

Hayashi, Y., Kashiwagi, M., Yasuda, K., Ando, R., Kanuka, M., Sakai, K., et al., 2015. Cells of a common developmental origin regulate REM/non-REM sleep and wakefulness in mice. Science 350 (6263), 957–961.

Hobson, J.A., McCarley, R.W., Wyzinski, P.W., 1975. Sleep cycle oscillation: reciprocal discharge by two brainstem neuronal groups. Science 189 (4196), 55–58.

Horner, R.L., Sanford, L.D., Annis, D., Pack, A.I., Morrison, A.R., 1997. Serotonin at the laterodorsal tegmental nucleus suppresses rapid-eye-movement sleep in freely behaving rats. J. Neurosci. 17 (19), 7541–7552.

Jouvet, M., 1962. Research on the neural structures and responsible mechanisms in different phases of physiological sleep. Arch. Ital. Biol. 100, 125–206.

Kádár, A., Wittmann, G., Liposits, Z., Fekete, C., 2009. Improved method for combination of immunocytochemistry and Nissl staining. J. Neurosci. Meth. 184, 115–118.

Kia, H.K., Miquel, M.C., Brisorgueil, M.J., Daval, G., Riad, M., El Mestikawy, S., et al., 1996. Immunocytochemical localization of serotonin1A receptors in the rat central nervous system. J. Comp. Neurol. 365 (2), 289–305.

Kohara, K., Pignatelli, M., Rivest, A.J., Jung, H.Y., Kitamura, T., Suh, J., Frank, D., Kajikawa, K., Mise, N., Obata, Y., Wickersham, I.R., Tonegawa, S., 2014. Cell type-specific genetic and optogenetic tools reveal hippocampal CA2 circuits. Nat. Neurosci. 17, 269–279.

Leonard, C.S., Llinás, R., 1994. Serotonergic and cholinergic inhibition of mesopontine cholinergic neurons controlling REM sleep: an in vitro electrophysiological study. Neuroscience 59 (2), 309–330.

Lin, J.S., 2000. Brain structures and mechanisms involved in the control of cortical activation and wakefulness, with emphasis on the posterior hypothalamus and histaminergic neurons. Sleep Med. Rev. 4 (5), 471–503.

Loucif, A.J.C., Bonnavion, P., Macri, B., Golmard, J.L., Boni, C., Melfort, M., Leonard, G., Lesch, K.P., Adrien, J., Jacquin, T.D., 2006. Gender-dependent regulation of G-protein-gated inwardly rectifying potassium current in dorsal raphe neurons in knock-out mice devoid of the 5-hydroxytryptamine transporter. J. Neurobiol. 66, 1475–1488.

Lu, J., Sherman, D., Devor, M., Saper, C.B., 2006. A putative flip-flop switch for control of REM sleep. Nature 441 (7093), 589–594.

Luebke, J.I., Greene, R.W., Semba, K., Kamondi, A., McCarley, R.W., Reiner, P.B., 1992. Serotonin hyperpolarizes cholinergic low-threshold burst neurons in the rat laterodorsal tegmental nucleus in vitro. Proc. Natl. Acad. Sci. U. S. A. 89 (2), 743–747.

Maudhuit, C., Jolas, T., Lainey, E., Hamon, M., Adrien, J., 1994. Effects of acute and chronic treatment with amoxapine and cericlamine on the sleep-wakefulness cycle in the rat. Neuropharmacology 33 (8), 1017–1025.

McGinty, D.J., Harper, R.M., 1976. Dorsal raphe neurons: depression of firing during sleep in cats. Brain Res. 101 (3), 569–575.

Mebatsion, T., Konig, M., Conzelmann, K.K., 1996. Budding of rabies virus particles in the absence of the spike glycoprotein. Cell 84, 941–951.

Monaca, C., Boutrel, B., Hen, R., Hamon, M., Adrien, J., 2003. 5-$HT_{1A/1B}$ receptor-mediated effects of the selective serotonin reuptake inhibitor, citalopram, on sleep: studies in 5-HT_{1A} and 5-HT_{1B} knockout mice. Neuropsychopharmacology 28 (5), 850–856.

Monti, J.M., Jantos, H., 2003. Differential effects of the 5-HT_{1A} receptor agonist flesinoxan given locally or systemically on REM sleep in the rat. Eur. J. Pharmacol. 478 (2–3), 121–130.

Muzerelle, A., Scotto-Lomassese, S., Bernard, J.F., Soiza-Reilly, M., Gaspar, P., 2016. Conditional anterograde tracing reveals distinct targeting of individual serotonin cell groups (B5-B9) to the forebrain and brainstem. Brain Struct. Funct. 221 (1), 535–561.

Panula, P., Yang, H.Y., Costa, E., 1984. Histamine-containing neurons in the rat hypothalamus. Proc. Natl. Acad. Sci. U. S. A. 81 (8), 2572–2576.

Pedersen, N.P., Ferrari, L., Venner, A., Wang, J.L., Abbott, S.B.G., Vujovic, N., Arrigoni, E., Saper, C.B., Fuller, P.M., 2017. Supramammillary glutamate neurons are a key node of the arousal system. Nat. Commun. 8.

Peyrache, A., Lacroix, M.M., Petersen, P.C., Buzsáki, G., 2015. Internally organized mechanisms of the head direction sense. Nat. Neurosci. 18 (4), 569–575.

Portas, C.M., Thakkar, M., Rainnie, D., McCarley, R.W., 1996. Microdialysis perfusion of 8-hydroxy-2-(di-n-propylamino)tetralin (8-OH-DPAT) in the dorsal raphe nucleus decreases serotonin release and increases rapid eye movement sleep in the freely moving cat. J. Neurosci. 16 (8), 2820–2828.

Portas, C.M., Bjorvatn, B., Ursin, R., 2000. Serotonin and the sleep/wake cycle: special emphasis on microdialysis studies. Prog. Neurobiol. 60 (1), 13–35.

Portas, C., Grønli, J., 2008. Involvement of the 5-HT_{1A} and the 5-HT_{1B} receptor in the regulation of sleep and waking. In: Monti, J.M., Pandi-Perumal, S.R., Jacobs, B.L., Nutt, D.J. (Eds.), Serotonin and Sleep: Molecular, Functional and Clinical Aspects. Birkhäuser Basel, pp. 325–369.

Rasmussen, K., Heym, J., Jacobs, B.L., 1984. Activity of serotonin-containing neurons in nucleus centralis superior of freely moving cats. Exp. Neurol. 83 (2), 302–317.
Riad, M., Garcia, S., Watkins, K.C., Jodoin, N., Doucet, E., Langlois, X., et al., 2000. Somatodendritic localization of 5-HT_{1A} and preterminal axonal localization of 5-HT_{1B} serotonin receptors in adult rat brain. J. Comp. Neurol. 417 (2), 181–194.
Sahly, I., Fabre, V., Vyas, S., Milet, A., Rouzeau, J.D., Hamon, M., et al., 2007. 5-HT1A-iCre, a new transgenic mouse line for genetic analyses of the serotonergic pathway. Mol. Cell. Neurosci. 36 (1), 27–35.
Sakai, K., 2011. Sleep-waking discharge profiles of dorsal raphe nucleus neurons in mice. Neuroscience 197, 200–224.
Sakai, K., Crochet, S., 2001. Role of dorsal raphe neurons in paradoxical sleep generation in the cat: no evidence for a serotonergic mechanism. Eur. J. Neurosci. 13 (1), 103–112.
Sakai, K., El Mansari, M., Lin, J.S., Zhang, J.G., Vanni Mercier, G., 1990. The posterior hypothalamus in the regulation of wakefulness and paradoxical sleep. In: Mancia, M., Marini, G. (Eds.), The Diencephalon and Sleep. Raven Press, New York, pp. 171–198.
Sanford, L.D., Tejani-Butt, S.M., Ross, R.J., Morrison, A.R., 1996. Elicited PGO waves in rats: lack of 5-HT_{1A} inhibition in putative pontine generator region. Pharmacol. Biochem. Behav. 53 (2), 323–327.
Saunders, R.C., Vann, S.D., Aggleton, J.P., 2012. Projections from Gudden's tegmental nuclei to the mammillary body region in the cynomolgus monkey (Macaca fascicularis). J. Comp. Neurol. 520 (6), 1128–1145.
Sharp, P.E., Tinkelman, A., Cho, J., 2001. Angular velocity and head direction signals recorded from the dorsal tegmental nucleus of Gudden in the rat: implications for path integration in the head direction cell circuit. Behav. Neurosci. 115 (3), 571–588.
Shibata, H., 1987. Ascending projections to the mammillary nuclei in the rat: a study using retrograde and anterograde transport of wheat germ agglutinin conjugated to horseradish peroxidase. J. Comp. Neurol. 264 (2), 205–215.
Slater, I.H., Jones, G.T., Moore, R.A., 1978. Inhibition of REM sleep by fluoxetine, a specific inhibitor of serotonin uptake. Neuropharmacology 17 (6), 383–389.
Sommerfelt, L., Hauge, E.R., Ursin, R., 1987. Similar effect on REM sleep but differential effect on slow wave sleep of the two 5-HT uptake inhibitors zimeldine and alaproclate in cats and rats. J. Neural. Transm. 68 (1–2), 127–144.
Sotelo, C., Cholley, B., El Mestikawy, S., Gozlan, H., Hamon, M., 1990. Direct Immunohistochemical evidence of the existence of 5-HT_{1A} autoreceptors on serotoninergic neurons in the midbrain raphe nuclei. Eur. J. Neurosci. 2 (12), 1144–1154.
Steininger, T.L., Alam, M.N., Gong, H., Szymusiak, R., McGinty, D., 1999. Sleep-waking discharge of neurons in the posterior lateral hypothalamus of the albino rat. Brain Res. 840 (1–2), 138–147.
Takahashi, K., Lin, J.S., Sakai, K., 2006. Neuronal activity of histaminergic tuberomammillary neurons during wake-sleep states in the mouse. J. Neurosci. 26 (40), 10292–10298.
Taube, J.S., 2007. The head direction signal: origins and sensory-motor integration. Annu. Rev. Neurosci. 30, 181–207.
Thakkar, M.M., Strecker, R.E., McCarley, R.W., 1998. Behavioral state control through differential serotonergic inhibition in the mesopontine cholinergic nuclei: a simultaneous unit recording and microdialysis study. J. Neurosci. 18 (14), 5490–5497.
Tissier, M.H., Lainey, E., Fattaccini, C.M., Hamon, M., Adrien, J., 1993. Effects of ipsapirone, a 5-HT_{1A} agonist, on sleep/wakefulness cycles: probable postsynaptic action. J. Sleep Res. 2 (2), 103–109.
Vanni-Mercier, G., Gigout, S., Debilly, G., Lin, J.S., 2003. Waking selective neurons in the posterior hypothalamus and their response to histamine H3-receptor ligands: an electrophysiological study in freely moving cats. Behav. Brain Res. 144 (1–2), 227–241.
Viereckel, T., Dumas, S., Smith-Anttila, C.J., Vlcek, B., Bimpisidis, Z., Lagerström, M.C., Konradsson-Geuken, Å., Wallén-Mackenzie, Å., 2016. Midbrain gene screening identifies a new mesoaccumbal glutamatergic pathway and a marker for dopamine cells neuroprotected in Parkinson's disease. Sci. Rep. 6, 35203.
Weber, F., Chung, S., Beier, K.T., Xu, M., Luo, L., Dan, Y., 2015. Control of REM sleep by ventral medulla GABAergic neurons. Nature 526 (7573), 435–438.
Wirtshafter, D., Stratford, T.R., 1993. Evidence for GABAergic projections from the tegmental nuclei of Gudden to the mammillary body in the rat. Brain Res. 630 (1–2), 188–194.